

# Kernel Choice Matters for Boundary Inference Using Local Polynomial Density: With Application to Manipulation Testing

Shunsuke Imai\* and Yuta Okamoto<sup>†‡</sup>

Graduate School of Economics, Kyoto University<sup>§</sup>

January 30, 2024

## Abstract

The local polynomial density (LPD) estimator has been a useful tool for inference concerning boundary points of density functions. While it is commonly believed that kernel selection is not crucial for the performance of kernel-based estimators, this paper argues that this does not hold true for LPD estimators at boundary points. We find that the commonly used kernels with compact support lead to larger asymptotic and finite-sample variances. Furthermore, we present theoretical and numerical evidence showing that such unfavorable variance properties negatively affect the performance of manipulation testing in regression discontinuity designs, which typically suffer from low power. Notably, we demonstrate that these issues of increased variance and reduced power can be significantly improved just by using a kernel function with unbounded support. We recommend the use of the spline-type kernel (the Laplace density) and illustrate its superior performance.

*Keywords:* local polynomial smoothing, kernel selection, efficiency, finite sample theory, regression discontinuity designs

---

\*[imai.shunsuke.57n@st.kyoto-u.ac.jp](mailto:imai.shunsuke.57n@st.kyoto-u.ac.jp)

<sup>†</sup>[okamoto.yuuta.57w@st.kyoto-u.ac.jp](mailto:okamoto.yuuta.57w@st.kyoto-u.ac.jp) (corresponding author)

<sup>‡</sup>We are indebted to our supervisors, Yoshihiko Nishiyama, Shin Kanaya, and Takahide Yanagi, for their guidance and support. We gratefully acknowledge Yasuyuki Hamura, Marc Henry, Takuya Ishihara, Yuuki Ozaki, Masayuki Sawada, and seminar/conference participants at Kyoto University, EcoSta 2023, and the 2023 Kansai Econometrics Meeting for their invaluable comments and suggestions. We wish to thank Ryo Inage for his code review. Okamoto is grateful for financial support from JST SPRING, Grant Number JPMJSP2110.

<sup>§</sup>606-8501, Yoshida-honmachi, Sakyo, Kyoto, Japan

# 1 Introduction

The probability density function at boundary points is often of interest in empirical analyses in economics, applied statistics, and many other fields of social and medical science. For example, the wage distribution on the lower tail is often important in several disciplines in social science (e.g., DiNardo et al., 1996), and empirical tests of economic theory are sometimes based on density at boundary points (e.g., Collin and Talbot, 2023). Another example is manipulation testing in regression discontinuity (RD) analysis, which examines the continuity of the density of the running variable at the threshold (Cattaneo and Titiunik, 2022; Cattaneo et al., 2023b).

Recently, a density estimator using the local polynomial kernel smoothing technique, called the local polynomial density (LPD) estimator, is proposed by Cattaneo et al. (2020). As they state, the LPD estimator “enjoys all the desirable features associated with local polynomial regression estimation,” including automatic boundary adaptation. Thanks to this better bias property, the LPD estimator is well used in manipulation testing in RD analysis as a primary application. The test has become a leading option, and many papers in empirical economics adopt it (e.g., Adams et al., 2022; Ayres et al., 2021; Britto et al., 2022; Chen et al., 2023; Connolly and Haeck, 2022; Dasgupta et al., 2022; Eggers et al., 2021; Gorrín et al., 2023; He et al., 2020; Kapoor et al., 2021; Khanna, 2023). Also, their methodology is accepted in other related fields (e.g., Kosec and Mo, 2023).

Despite its popularity, the LPD at the boundary does not exhibit good numerical performance in some cases. The following example illustrates this. In Figure 1, we generate “manipulated” data that has a discontinuous density and perform the LPD-based discontinuity test by following the recommended procedure in Cattaneo et al. (2020, 2018). As a result, the LPD exhibits unexpectedly large confidence intervals near the boundary point and the formal test cannot detect this relatively large discontinuity (Figure 1a). Nonetheless, such a problematic behavior seems to be improved if we use a different kernel function, as in Figure 1b; the confidence intervals are much sharper and do not overlap, and the formal test successfully detects the discontinuity just by changing the kernel function.

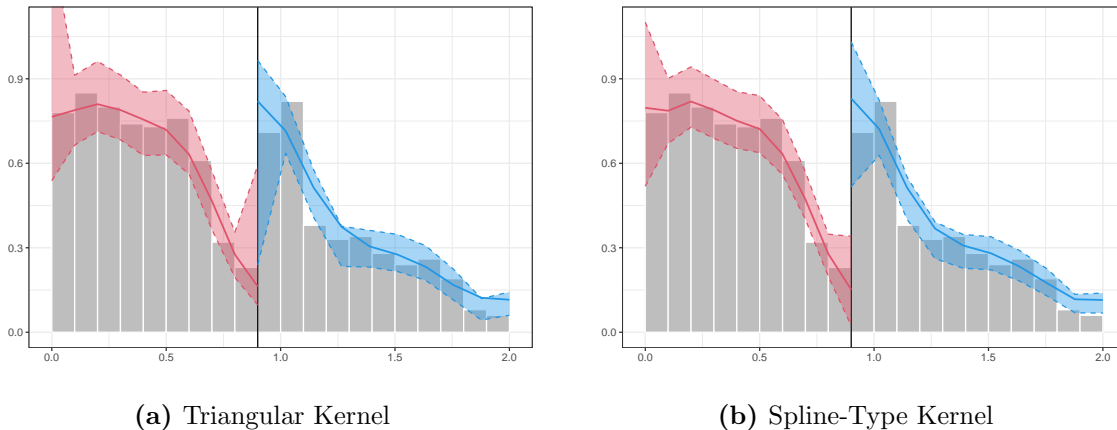


**Figure 1:** Manipulated Data and Discontinuity Test. *The vertical line indicates the cutoff.*

In this paper, we show that the problematic phenomena (Figure 1a) and the improvement

(Figure 1b) are explained by both the asymptotic and finite-sample variance properties of the LPD estimator that are indeed derived from the kernel function. We will firstly see that the asymptotic efficiency non-trivially depends on the kernel choice, contrary to what is usually assumed. In particular, the LPD estimator with commonly used kernel functions with compact support has a significantly larger asymptotic variance than the so-called spline-type kernel with non-compact support at boundaries, which leads to a non-negligible efficiency loss. In addition, we show that the LPD estimator inherits not only the “desirable features” of local polynomial techniques but also an *undesirable* finite-sample property of having no finite variance when a compactly supported kernel is used (Seifert and Gasser, 1996).

These undesirable variance properties are carried over to a manipulation test for RD designs and possibly make the power low. Besides, the unique property of manipulation that the sample size decreases on one side of the cutoff can increase variance, thereby makes the situation worse: Even with a large discontinuity, the power does not necessarily improve due to the inflated variance; furthermore, when the degree of manipulation is extreme, the finite-sample variance property may become dominant in that region with few observations, leading to a deterioration of the discontinuity test. These problematic properties of the LPD-based manipulation test make it often fail to reject the density’s continuity at the cutoff when commonly used kernels are employed, whereas we will show that this lack of power can be largely improved just by changing kernel function as we have seen above.

These theoretical and numerical investigations suggest that the non-compactly supported kernel function, such as the spline-type kernel, is preferable, and hence, we propose to use this kernel rather than commonly employed ones in boundary inference using the LPD estimator. This remedy is simple but powerful. The amount of improvement in efficiency, power, and numerical performance is drastic.

## Plan of the Article

This paper is organized as follows. In the remainder of this section, we introduce the LPD estimator, some known results provided in Cattaneo et al. (2020), and also some notation. Section 2 discusses the general variance properties of LPD and considers why kernel choice is important. In Section 3, we treat the manipulation testing in RD designs, whose unique feature highlights the importance of kernel selection. Several numerical and empirical analyses are also performed. Section 4 concludes this paper. Proofs, additional simulation and empirical results, and additional theoretical arguments are collected in the Online Appendix.

## Setup and Notation

Let  $\mathcal{X} = (-\infty, x_R) \subseteq \mathbb{R}$  be the data domain. We are given independent and identically distributed samples  $X_{1:n} = (X_1, \dots, X_n)$  defined on  $\mathcal{X}$  with unknown distribution  $F$  and density  $f$ . Assume that we are interested in the density at the boundary, i.e.,  $f(x_R)$ . The

LPD estimator of [Cattaneo et al. \(2020\)](#) at the boundary point  $x_R$  is given by

$$\begin{aligned}\hat{f}(x_R) &= \mathbf{e}'_1 \hat{\boldsymbol{\beta}}(x_R), \\ \hat{\boldsymbol{\beta}}(x_R) &= \arg \min_{\boldsymbol{\beta} \in \mathbb{R}^{p+1}} \sum_{i=1}^n \left\{ \hat{F}(X_i) - \mathbf{r}_p(X_i - x_R)' \boldsymbol{\beta} \right\}^2 \frac{1}{h} K \left( \frac{X_i - x_R}{h} \right),\end{aligned}\quad (1.1)$$

where  $\mathbf{e}_1 = (0, 1, 0, \dots, 0)'$ ,  $\hat{F}(x) = n^{-1} \sum_{i=1}^n \mathbf{1}\{X_i \leq x\}$ ,  $\mathbf{r}_p(u) = (1, u, u^2, \dots, u^p)'$ ,  $K(\cdot)$  is a non-negative, symmetric kernel function such that  $\int K(u) du = 1$ ,  $h$  is a bandwidth such that  $h \rightarrow 0$  and  $nh \rightarrow \infty$ , and  $p(\geq 1)$  is the polynomial degree.

The asymptotic bias and variance of  $\hat{f}(x_R)$  are obtained under standard assumptions in [Cattaneo et al. \(2020, p.1451\)](#) as  $f^{(p)}(x_R)/\{(p+1)!\} \times \mathcal{B}_{p,K}$  and  $f(x_R) \times \mathcal{V}_{p,K}$ , respectively, where  $\mathcal{B}_{p,K} = \mathbf{e}'_1 \mathbf{A}_{p,K}^{-1} \mathbf{c}_{p,K}$ ,  $\mathcal{V}_{p,K} = \mathbf{e}'_1 \mathbf{A}_{p,K}^{-1} \mathbf{B}_{p,K} \mathbf{A}_{p,K}^{-1} \mathbf{e}_1$ , with

$$\begin{aligned}\mathbf{A}_{p,K} &= \int_{-\infty}^0 \mathbf{r}_p(u) \mathbf{r}_p(u)' K(u) du, & \mathbf{c}_{p,K} &= \int_{-\infty}^0 \mathbf{r}_p(u) u^{p+1} K(u) du, \\ \mathbf{B}_{p,K} &= \int_{-\infty}^0 \int_{-\infty}^0 \min\{u, v\} \mathbf{r}_p(u) \mathbf{r}_p(v)' K(u) K(v) dudv.\end{aligned}\quad (1.2)$$

The (asymptotic) mean squared error (MSE) optimal bandwidth can be deduced from these that

$$h_p^{\text{MSE}} = \left( \frac{\mathcal{V}_{p,K}}{C_1(p, x_R, F) \mathcal{B}_{p,K}^2} \right)^{1/(2p+1)} n^{-1/(2p+1)},$$

where  $C_1(p, x_R, F)$  is some constant that depends only on  $p$ ,  $x_R$ , and  $F$  ([Cattaneo et al., 2020, p.1452](#)).

In what follows, we write a positive part of a function  $g$  by  $(g)_+$  or  $\{g\}_+$  and a negative part by  $(g)_-$  or  $\{g\}_-$ . The support of  $g$  is denoted by  $\text{supp}(g)$ .

## 2 Why Kernel Choice Matters

In [Section 2.1](#) and [2.2](#), we respectively investigate how much and why kernel choice is important for the LPD estimator.

### 2.1 Asymptotic Efficiency

Thanks to the asymptotic bias and variance expression above, we can study the dependence of the asymptotic variance and asymptotic MSE on kernel functions through  $\mathcal{V}_{p,K}$  and  $\mathcal{Q}_{p,K}$ , which is given by

$$\mathcal{Q}_{p,K} = (\mathcal{B}_{p,K}^2)^{1/(2p+1)} \mathcal{V}_{p,K}^{2p/(2p+1)},$$

since  $\text{MSE}(h_p^{\text{MSE}}) \approx \mathcal{Q}_{p,K} \times C_2 n^{-2p/(2p+1)}$  with some constant  $C_2$  that does not depend on  $K$ .

Kernel Function	$\mathcal{V}_{p,K}$			$\mathcal{Q}_{p,K}$		
	$\mathcal{V}_{1,K}$	$\mathcal{V}_{2,K}$	$\mathcal{V}_{3,K}$	$\mathcal{Q}_{1,K}$	$\mathcal{Q}_{2,K}$	$\mathcal{Q}_{3,K}$
Triangular	1.37143 (5.49)	5.71429 (7.62)	14.026 (9.97)	1.06376 (1.06)	2.87329 (1.14)	5.9886 (1.21)
Uniform	1.2 (4.80)	5.48571 (7.31)	14.2857 (10.16)	1.12924 (1.13)	3.18161 (1.26)	6.83074 (1.38)
Epanechnikov	1.34547 (5.38)	5.77201 (7.70)	14.4678 (10.29)	1.08683 (1.09)	2.99072 (1.18)	6.32592 (1.28)
Gaussian	0.483582 (1.93)	1.7485 (2.33)	3.80874 (2.71)	1.0408 (1.04)	2.73937 (1.08)	5.56648 (1.13)
Spline	0.25 (1.00)	0.75 (1.00)	1.40625 (1.00)	1 (1.00)	2.5244 (1.00)	4.93485 (1.00)

**Table 1:** Asymptotic Variance and Efficiency Relative to the Spline Kernel. We show  $\mathcal{V}_{p,K}$  and  $\mathcal{Q}_{p,K}$ . The numbers in parentheses indicate the relative variance and efficiency compared to the spline kernel.

Based on these  $\mathcal{V}_{p,K}$  and  $\mathcal{Q}_{p,K}$ , we compare several kernel functions with respect to their relation to the asymptotic behavior; in particular, we use the triangular  $((1 - |u|)_+)$ , uniform  $(\mathbf{1}\{u^2 < 1\}/2)$ , Epanechnikov  $(3/4 \cdot (1 - u^2)_+)$ , Gaussian  $(\exp(-u^2/2)/\sqrt{2\pi})$ , and spline-type  $(\exp(-|u|)/2)$  kernels. The first three kernels are the popular choice and are compactly supported. The other two kernels are non-compactly supported. For the reason why we may focus our attention on these five kernels, see Appendix A and Remark 1 below. We denote the class of kernel functions comprising these five by  $\mathcal{K}$ .

The asymptotic variance ( $\mathcal{V}_{p,K}$ ) and MSE-efficiency ( $\mathcal{Q}_{p,K}$ ) for these kernels in  $\mathcal{K}$  and  $p = 1, 2, 3$  are summarized in Table 1. We can see that the non-compactly supported kernels in  $\mathcal{K}$  achieve better variance and efficiency properties than the commonly used kernels with compact support. Notice also that, unlike usual, the kernel choice has a non-trivial impact on the asymptotic MSE-efficiency; for the case when  $p = 2$ , which is the most standard choice in the literature (Cattaneo et al., 2020, p.1452; Fan and Gijbels, 1996, pp.76-80), the compactly supported kernels are 14-26% less efficient than the spline-type kernel. Intuitively speaking, it implies that the commonly used kernels require around 1.2-1.3 times larger sample size to achieve the same performance as the spline-type kernel. Besides, in fact, such an efficiency loss is much more severe in inference, as we will see later.

## 2.2 Why Kernel Choice Matters: Equivalent Kernel Perspective

This subsection investigates the reason why the kernel choice has a nontrivial impact on the efficiency of the LPD. Our discussion relies on the equivalent kernel (Fan and Gijbels, 1996, p.63), which is useful for understanding how the LPD applies weights to each datum point. The LPD estimator can be rewritten by

$$\hat{f}(x_R) = \frac{1}{nh} \sum_{i=1}^n \int_{-\infty}^0 \mathbf{e}'_i \mathbf{A}_{p,K}^{-1} \mathbf{r}_p(u) K(u) \mathbf{1} \left\{ \frac{X_i - x_R}{h} \leq u \right\} du + o_p(1).$$

See Section S1.2 in the Supplementary Materials for the derivation. This expression suggests that the LPD estimator at boundary points is asymptotically equivalent to the standard

kernel density estimator (KDE) using the following (asymmetric) kernel function,

$$K_{p,K}^*(u) = \int_{-\infty}^0 \mathbf{e}'_1 \mathbf{A}_{p,K}^{-1} \mathbf{r}_p(z) K(z) \mathbf{1}\{u \leq z\} dz. \quad (2.1)$$

Therefore, an investigation of  $K_{p,K}^*$  will provide insights into how the LPD utilizes the information contained within the sample. The following proposition characterizes the basic properties of  $K_{p,K}^*$  and will play an important role in understanding the variance property.

**Proposition 1.** *Assume  $K$  is symmetric, everywhere nonnegative second-order kernel function such that*

$$\int_0^\infty u^{2p} K(u) du < \infty.$$

*Then it holds that  $\text{supp}(K_{p,K}^*) = \text{supp}(K) \cap (-\infty, 0]$ ,  $K_{p,K}^*(0) = 0$ , and*

$$\int_{-\infty}^0 u^j K_{p,K}^*(u) du = \delta_{0,j} \quad (0 \leq j \leq p-1), \quad (2.2)$$

*where  $\delta_{0,j}$  takes 1 if  $j = 0$  and 0 otherwise.* ♣

Therefore, the equivalent kernel  $K_{p,K}^*$  is the  $p$ -th order boundary kernel that satisfies the moment conditions of Gasser et al. (1985, p.244), which reflects that the LPD estimator is boundary adaptive. The property of  $K_{p,K}^*(0) = 0$  arises from our use of  $\hat{F}$  as the “dependent variable.” At the boundary,  $\hat{F}(x_R) - \mathbf{r}_p(0)' \hat{\boldsymbol{\beta}}$  shrinks very quickly (Cattaneo et al., 2020, Supplemental Appendix), eliminating its contribution to the loss in (1.1). As a result, the LPD asymptotically does not use information from the data at the boundary.

To understand the variance property, the moment conditions in (2.2) and  $K_{p,K}^*(0) = 0$  are crucial. Notice firstly that  $K_{p,K}^*$  integrates to one, but its higher moments are zero. This fact implies that  $K_{p,K}^*$  necessarily has to take negative values. Recalling that  $K_{p,K}^*(0) = 0$ , it will become apparent that  $K_{p,K}^*$  has to rise from the origin and then descend to negative values, forming a valley (see Figure 2). Now, recall that when a compactly supported kernel is employed,  $K_{p,K}^*$  is also compactly supported, since  $\text{supp}(K_{p,K}^*) \subset \text{supp}(K)$ . Then, as a result, when  $K$  is compactly supported,  $K_{p,K}^*$  has to produce a large valley and a resulting sharp fluctuation to meet both the moment conditions and the support condition. This “roughness” due to the fluctuation will contribute to the large variance, considering that the asymptotic variance for KDE is proportional to  $\int K^2$ . In contrast, this kind of large fluctuation will not happen if  $K$  is non-compactly supported because  $K_{p,K}^*$  can now change its shape more flexibly over its tail. Figure 2 showcases this observation using the triangular and spline-type kernel with  $p = 2$ . The equivalent kernels  $K_{2,K}^*$  are shown in Figure 2a, in which we can see that the triangular kernel exhibits a deep valley, whereas the spline-type kernel does not and shows smooth skirt. These observations clearly illustrate why the asymptotic variance is larger for the compactly supported kernels.

In Figure 2b, we show these equivalent kernels that are scaled to have the same asymptotic variance ( $\mathcal{V}_{2,K}$ ). We can see that the negative region is much more modest for the spline-type kernel than the triangular kernel. This suggests that  $\int u \{K_{p,K}^*(u)\}_-$  is much smaller for the

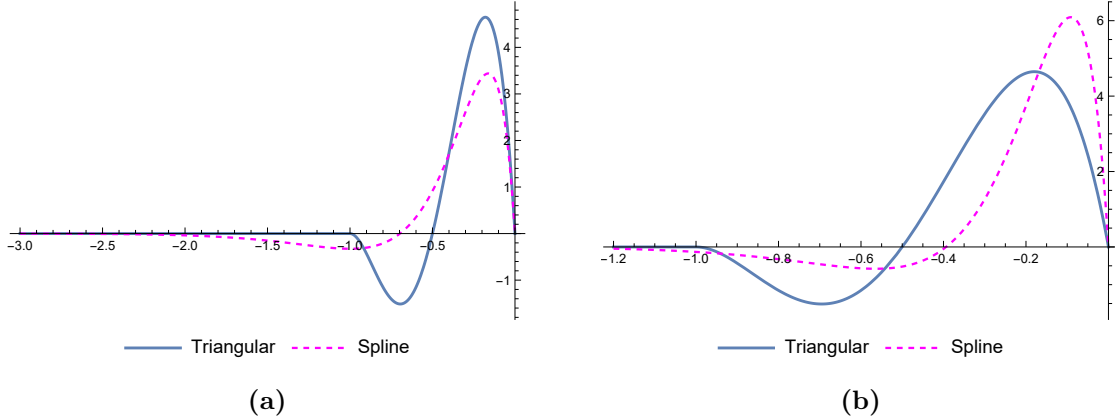


**Figure 2:** Equivalent Kernels of the Triangular and Spline Kernel.  $K_{2,K}^*$  of the spline kernel is scaled so that both have the same  $\int u\{K_{2,K}^*(u)\}_+$  in Panel (a) and the same asymptotic variance in Panel (b).

spline-type kernel, and as a consequence,  $\int u\{K_{p,K}^*(u)\}_+$  is also smaller (in the absolute value sense). This indicates that  $K_{p,K}^*$  can take larger values where  $|u|$  is small. This means that the spline-type kernel assigns larger weights near the right boundary (i.e., the evaluation point), which successfully reduces bias. This illustrates why non-compactly supported kernels in  $\mathcal{K}$  dominate compactly supported ones in the MSE sense.

These illustrations explain why the non-compactly supported kernels, such as the Gaussian and spline-type kernels, dominate the popular kernels with compact support in Table 1. Besides, although employing non-compactly supported kernels is counter-intuitive as they seem to “use” the datum point far away from the evaluation point at first glance, the analysis above suggests the non-compactness rather makes it possible to apply more weight near the evaluation point, improving the intuitive appropriateness of such weighting scheme.

Our analysis above also offers a new insight into the standard KDE at (and near) boundary points. The classical literature, such as Müller (1991) and Gasser et al. (1985), restrict their attention only to compactly supported kernels to obtain an “optimal” kernel with no theoretical backing. In fact, Müller’s preferred “near-optimal” kernel among compactly supported kernels (see Müller, 1991, lines 13-31 on p.524 and section 3) coincides with the equivalent kernel of the LPD estimator with the uniform kernel, but we know by Table 1 that the equivalent kernel of the spline-type kernel is much more MSE-efficient. This suggests that relaxing this compact-support condition in KDE at boundaries will lead to a further MSE-efficiency gain. This efficiency improvement by employing non-compactly supported kernels is new or overlooked in the literature, and it is in contrast to the KDE at interior points, in which the MSE-optimal kernel is the best among non-negative kernels, not only among compactly supported kernels (Gasser et al., 1985; Granovsky and Müller, 1991). In addition, the formula for the equivalent kernel (2.1) provides a new strategy to construct a boundary kernel function. For example, the equivalent kernel of the spline-type kernel,  $-\exp(u)u(3+u)$ , is novel to the literature, to our best knowledge.

**Remark 1.** The discussion above suggests that spline-type kernel is a good choice not only among the kernels in  $\mathcal{K}$ . Firstly, from the perspective of the existence of moments



( $\int u^k K(u) du$ ), the exponentially decaying functions are natural candidates. Here, if the tail decay becomes faster, it approaches a more compactly supported function, which worsens the variance property (e.g., the Gaussian kernel). Therefore, the Laplace density (i.e., the spline-type kernel), which has a gentler tail decay, is appropriate as a kernel for the boundary estimation using the LPD. In the Online Appendix (Table S1), we also construct some kernel functions whose tails decay faster than the Gaussian kernel and slower than the spline-type kernel and show that they are less efficient than the spline-type kernel.  $\lrcorner$

### 2.3 Finite Sample Variance Properties

So far, we have investigated how the variance property depends on the kernel function in the asymptotic sense. In this subsection, we again study the effect of kernel selection on the estimation accuracy but in the *non-asymptotic* sense. Concretely, we will theoretically show that the finite-sample variance of the LPD estimator cannot be bounded if we use compactly supported kernels.

We start with a heuristic explanation of why the variance inflates as it is more intuitive and the essence is not so different from our rigorous proof. Assume that the kernel function is compactly supported and fix  $h$  and  $p$ . Then, using the law of total variance, we can obtain the lower bound of the finite-sample variance as follows:

$$\begin{aligned} \mathbb{V} \left[ \hat{f}(x_R) \right] &\geq \mathbb{E} \left[ \mathbb{V} \left[ \hat{f}(x_R) \mid \mathbf{1} \{n_0 \leq p + 2\} \right] \right] \\ &\geq \mathbb{V} \left[ \hat{f}(x_R) \mid \mathbf{1} \{n_0 \leq p + 2\} = 1 \right] \times \underbrace{\mathbb{P} [n_0 \leq p + 2]}_{>0}, \end{aligned} \quad (2.3)$$

where  $n_0$  is the local sample size around the boundary point  $x_R$ , that is, the number of observations in  $[x_R - h, x_R)$ . Here, note that the estimator can be understood as a coefficient of the standard regression model on  $[x_R - h, x_R)$ . Then, we can deduce from the classic linear regression theory (see [Kinal, 1980](#); [Hansen, 2022](#), pp.103-104) that

$$\mathbb{V} \left[ \hat{f}(x_R) \mid \mathbf{1} \{n_0 \leq p + 2\} = 1 \right] = \mathbb{V} \left[ \hat{f}(x_R) \mid n_0 \leq p + 2 \right] = \infty.$$

This immediately implies that the (finite sample) variance of the LPD estimator diverges, or  $\mathbb{V} \left[ \hat{f}(x_R) \right] = \infty$ . The following theorem restates this intuition formally. Our result relies on the next assumptions.

**Assumption 1.** *The kernel function is non-negative and compactly supported.*

**Assumption 2.**  *$f(x)$  is supported by a bounded region,  $\mathcal{S} = [x_L, x_R)$ , and  $0 < \delta \leq f(x) \leq \Delta < \infty$  on  $\mathcal{S}$ .*

**Assumption 3.** *There exists no tie in  $X_{1:n}$ .*

Assumptions 2 and 3 are made to simplify the proof, but are still standard. We note that Assumption 3 holds with probability one when  $f$  is continuous. Under these assumptions, we have the next theorem:



**Theorem 1.** *Under Assumptions 1, 2, and 3, the LPD estimator  $\hat{f}(x_R)$  of degree  $p = 1$  does not have a second moment.* ♣

**Remark 2.** The statement should also hold for  $p \geq 2$ , as the variance will inflate as the number of parameters to be estimated increases in general. To prove this formally requires an algebraic effort, but we provide proof for the case when  $p = 2$  in the Online Appendix so as to illustrate that the essential problem is the same. ▽

Theorem 1 states that we cannot have a bounded variance of the LPD estimator. This would be a crucial problem in practice, as we always have (only) finite samples.

In essence, the finite-sample behavior derives from the sparsity relative to the polynomial order (or the small degree of freedom) and the resulting overfitting. To better understand this point, we can refer to (2.3). From the conditioning part in (2.3), we can deduce that the local sample size  $n_0$  relative to the polynomial degree  $p$  plays an important role. This intuition can be supported by the following argument: In the region where the sample size relative to the number of parameters is small, the model overly fits the data at hand. Then, the estimate becomes sensitive to the realization. In addition, importantly, the local polynomial fitting possibly yields an excessively large  $\hat{f}(x_R)$ , as the “slope” term can take an arbitrarily large value supposing the data are distributed quite closely in a sparse region. Then, the finite-sample variance inflates.

In this sense, the erratic behavior is not an LPD-specific problem but rather one that arises in the local polynomial fitting in general. In fact, Seifert and Gasser (1996) show that the finite-sample variance of the local linear regression estimator with a compactly supported kernel is infinite under a homoskedastic error assumption. In the Online Appendix, we show and discuss the theoretical connection between the LPD estimator and the local polynomial regression in detail, which clarifies that the root cause is the same for both estimators and provides another relevant insight into local polynomial fitting.

Now, we notice that a simple remedy for this negative result is available. The infinite variance problem does not arise if we use a non-compactly supported kernel, as the “local” sample size  $n_0$  is equal to the whole sample size  $n$ . Roughly speaking, when a kernel function is non-compactly supported, the LPD estimator can be seen as the usual weighted least squares (that uses the whole samples), and we can expect it to exhibit a much stabler behavior. Formally, we have the next result.

**Assumption 1’.** *The kernel function is positive everywhere, centralized at zero, and monotonically decreasing.*

**Theorem 1’.** *Assume  $n \geq 7$ . Under Assumptions 1’, 2, and 3, the LPD estimator  $\hat{f}(x_R)$  of degree  $p = 1$  has a second moment.*

Therefore, we can avoid the problematic behavior of the LPD estimator just by using non-compactly supported kernels such as the spline-type kernel. (The assumption  $n \geq 7$  could be slightly relaxed but is made as it enables us to prove the statement by a straightforward argument.)

### 3 Manipulation Testing

A primary application of the LPD is the manipulation testing for RD analysis. This test examines the continuity of the density function of the running variable at the cutoff  $x_R$ :

$$H_0 : \lim_{x \uparrow x_R} f(x) = \lim_{x \downarrow x_R} f(x) \text{ vs. } H_1 : \lim_{x \uparrow x_R} f(x) \neq \lim_{x \downarrow x_R} f(x).$$

In this section, we introduce [Cattaneo et al. \(2020\)](#)'s LPD-based test statistic and investigate why the variance reduction and kernel selection are important to improve the power of the test (Section 3.1-3.2). After that, in Section 3.3, we confirm by performing numerical experiments that the reduction in variance due to the kernel choice indeed and significantly increases the power.

#### 3.1 Power Function of LPD-Based Test Statistic

[Cattaneo et al. \(2020, Section 4\)](#) established a testing procedure based on their proposed LPD estimator and its validity. Let  $f_+(x_R) := \lim_{x \uparrow x_R} f(x)$  and  $f_-(x_R) := \lim_{x \downarrow x_R} f(x)$  and define their estimator  $\hat{f}_{p,+}(x_R)$  and  $\hat{f}_{p,-}(x_R)$  as the  $p$ -th order LPDs using only units with  $X_i \geq x_R$  and  $X_i \leq x_R$ , respectively. Their asymptotic variances can be written by  $f_+(x_R)\mathcal{V}_{+,p,K}$  and  $f_-(x_R)\mathcal{V}_{-,p,K}$ . Let  $\hat{\mathcal{V}}_{+,p,K}$  and  $\hat{\mathcal{V}}_{-,p,K}$  be their estimators and  $h_-$  and  $h_+$  denote the bandwidths used below and above  $x_R$ . Then, the LPD-based test statistic is defined as

$$T_p(h) := \frac{\frac{n_+}{n} \hat{f}_{p,+}(x_R) - \frac{n_-}{n} \hat{f}_{p,-}(x_R)}{\sqrt{\frac{n_+}{n} \frac{1}{nh_+} \hat{\mathcal{V}}_{+,p,K} + \frac{n_-}{n} \frac{1}{nh_-} \hat{\mathcal{V}}_{-,p,K}}}.$$

In the rest of this subsection, we explain that the variance has a major influence on the power. For the exposition, suppose the variance is known and we introduce the simpler expression of  $T_p(h)$  as  $\hat{\tau}/\sigma(\hat{\tau})$ , with  $\hat{\tau} = \frac{n_+}{n} \hat{f}_{p,+}(x_R) - \frac{n_-}{n} \hat{f}_{p,-}(x_R)$  and

$$\sigma(\hat{\tau}) = \sqrt{\frac{n_+}{n} \frac{1}{nh_+} f_+(x_R)\mathcal{V}_{+,p,K} + \frac{n_-}{n} \frac{1}{nh_-} f_-(x_R)\mathcal{V}_{-,p,K}}.$$

As in the case of usual tests, the variance has a dominating effect on the power. Under the alternative hypothesis with a fixed level of discontinuity  $|\tau| \neq 0$ , the power function is approximated as

$$\mathbb{P} \left( \left| \frac{\hat{\tau}}{\sigma(\hat{\tau})} \right| \geq \Phi_{1-\frac{\alpha}{2}}^{-1} \right) \approx 1 - \Phi \left( -\frac{\tau}{\sigma(\hat{\tau})} + \Phi_{1-\frac{\alpha}{2}}^{-1} \right) + \Phi \left( -\frac{\tau}{\sigma(\hat{\tau})} + \Phi_{\frac{\alpha}{2}}^{-1} \right).$$

Since  $\sigma^{-1}(\hat{\tau})|\tau| = O(n \max \{(n_+^{-1}h_+)^{1/2}, (n_-^{-1}h_-)^{1/2}\}) \rightarrow \infty$  while  $\Phi_q^{-1} = O(1)$  for every  $q \in (0, 1)$ ,  $\sigma^{-1}(\hat{\tau})\tau$  is dominant to  $\Phi_q^{-1}$ . Then, given the level of  $|\tau|$ , the discontinuity is more likely to be detected as  $\sigma(\hat{\tau})$  becomes smaller. Therefore, it is important to reduce the variance to improve the power.

Beyond this general property that applies to statistical tests, there are unique aspects of manipulation testing that give added importance to reducing variance. In typical tests, a

larger value of  $|\tau|$  may invariably lead to increased power, making the reduction of variance less critical when  $|\tau|$  is substantial. However, in the context of a manipulation test, this relationship does not always hold true. Specifically, in RD design settings, the occurrence of manipulation (say  $\tau > 0$ ) leads to the decreases in the sample size below the cutoff, due to the shift of some individuals across the cutoff as Figure 3 indicates. This manipulation-specific property can increase the variance  $\sigma(\hat{\tau})$  and consequently can reduce the power, although it cannot be determined whether this power loss is greater than the power increase due to the increase in  $|\tau|$  in general, of course. Furthermore, when the manipulation is extremely large, the sample size drops so significantly that it is necessary to pay attention to the finite-sample variance properties discussed in Section 2.3.

For the reasons mentioned above, it is essential to reduce the variance for a powerful manipulation test.

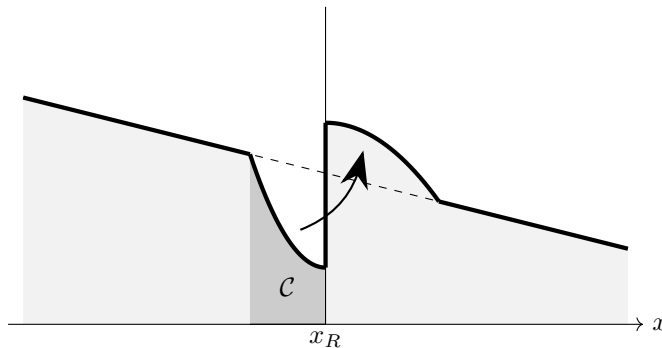


**Figure 3:** Manipulation and Sample Size around the Cut-Off. The thick line is the density of the running variable. The manipulation happens in the region  $\mathcal{C}$

### 3.2 Asymptotic Variance under Simple Robust Bias Correction

In this subsection, we briefly investigate how much  $\sigma(\hat{\tau})$  depends on the kernel function.

Cattaneo et al. (2020) proposed to use the test statistic  $T_3(h_2^{\text{MSE}})$  based on the simple robust bias correction idea (Calonico et al., 2014, Remark 7). In what follows, we analyze this test statistic, but also provide some additional remarks in the Online Appendix about the likely refinement attempts of  $T_3(h_2^{\text{MSE}})$  and their difficulties in view of its relation to the previous works on local polynomial smoothing, such as Calonico et al. (2018, 2020, 2022). These underscore the usefulness of our discussion on kernel selection.

We now proceed to the main analysis. With  $T_3(h_2^{\text{MSE}})$ , we can obtain that

$$\sigma^2(\hat{\tau}) \asymp \mathcal{V}_{3,K}/(nh_2^{\text{MSE}}) \approx \Theta_K \times C_3(f, x, p)n^{-4/5},$$

where  $\Theta_K = (\mathcal{B}_{2,K}^2)^{1/5} \mathcal{V}_{2,K}^{-1/5} \mathcal{V}_{3,K}$ . Therefore, we can study the dependence of  $\sigma(\hat{\tau})$  on  $K$  through  $\Theta_K$ . Figure 2 summarizes  $\Theta_K$  among the kernels in  $\mathcal{K}$ . We can see that the triangular kernel is approximately 50% less efficient than the spline-type kernel. Besides, the uniform kernel, which is also popular in empirical studies, exhibits much worse performance and is 75% less efficient. These values are worth noting. Roughly speaking, these kernels require 1.6 to 1.9 times larger sample size to achieve the same performance as the spline-type kernel

in terms of  $\sigma(\hat{\tau})$ . This implies that using such kernels can lead to significantly low power, and their use is not supportable from a theoretical viewpoint.

Kernel Function	Triangular	Uniform	Epanechnikov	Gaussian	Spline
$\Theta_K$	7.05261 (1.49)	8.28544 (1.75)	7.49635 (1.58)	5.96715 (1.26)	4.73325 (1.00)

**Table 2:** Asymptotic Variance and Efficiency Relative to the Spline Kernel. *We show  $\Theta_K$ . In the parentheses, we show its relative value to the spline kernel.*

### 3.3 Numerical Experiments

We now examine the power of manipulation testing based on the LPD estimator. We consider the following data-generating process and manipulation scheme.

1. Randomly generate  $N(\gg n)$  data from  $N(0, 1)$  and omit negatively valued data.
2. Pick  $n$  data (randomly).
3. Choose  $q \times 100\%$  of the data in  $(c, 0.9)$ ; and then replace them with  $0.9 + u_i$  where  $u_i \sim \text{Uniform}(0, \epsilon)$ .

That is, we consider the situation that some of the observations potentially in  $(c, 0.9)$  have moved to  $[0.9, 0.9 + \epsilon]$ , where 0.9 is the cutoff. We consider the following five cases: (1)  $q = 0.5, c = 0.8, \epsilon = 0.2$ , (2)  $q = 0.5, c = 0.8, \epsilon = 0.002$ , (3)  $q = 0.5, c = 0.7, \epsilon = 0.2$ , (4)  $q = 0.5, c = 0.7, \epsilon = 0.002$ , (5)  $q = 0.95, c = 0.7, \epsilon = 0.2$ , and (6) no-manipulation case, i.e., we stop at step 2. Note that a smaller  $c$  implies that the manipulation occurs over a larger region and a very small  $\epsilon$  suggests that the manipulators are concentrated at the cutoff, forming a poll in the density. Examples of the histogram for cases (1)-(6) are provided in the Online Appendix. Figure 1 in Section 1 corresponds to the case (3).

We perform the manipulation testing based on  $T_3(\hat{h}_2^{\text{MSE}})$  with samples  $n = 1000, 750$  and 500 for 2000 repetitions, respectively. The nominal level is set to be 0.05. We use the triangular kernel (default in Cattaneo et al., 2018), the Gaussian kernel, and the spline-type kernel. Conditions other than the kernel choice, such as bandwidth selection and standard error estimation, are mostly identical, and we follow the default settings of Cattaneo et al. (2018). The only difference is that we require the minimum number of observations in the bandwidth to be zero for non-compactly supported kernels. This modification is natural as they apply positive weights to the observations outside the bandwidth. However, we report the simulation results under the same set of options in the Online Appendix for transparency of the numerical results, which show qualitatively similar results.

The results are summarized in Table 3. We can observe several features that are consistent with previous sections. Firstly, the triangular kernel exhibits poor performance in many cases, especially when the “manipulators” do not form the pole (i.e., (1), (3), and (5)); in the worst case, the triangular kernel is only able to detect discontinuities approximately half of the time. Besides, the situation gets worse if  $n$  is smaller.

$n$	1000			750			500		
Kernel	Triangular	Gaussian	Spline	Triangular	Gaussian	Spline	Triangular	Gaussian	Spline
(1)	75.50	88.45	<b>96.10</b>	65.55	78.60	<b>90.65</b>	49.85	59.75	<b>73.50</b>
(2)	94.40	92.10	<b>97.30</b>	87.90	86.50	<b>93.85</b>	69.50	70.80	<b>82.65</b>
(3)	52.30	76.95	<b>94.95</b>	46.90	72.20	<b>92.10</b>	40.90	67.40	<b>87.15</b>
(4)	99.50	<b>100.00</b>	<b>100.00</b>	98.25	99.85	<b>100.00</b>	90.50	97.65	<b>99.95</b>
(5)	66.40	95.70	<b>100.00</b>	44.25	92.75	<b>99.85</b>	36.35	89.15	<b>98.75</b>
(6)	4.35	4.80*	4.60	4.15	4.45*	4.35	4.00	4.10*	4.05

**Table 3:** Rejection Rates (%). *The percentage of 2000 simulations with  $p$ -values below 0.05 is shown. The best for the with-manipulation cases are highlighted in bold blue. The closest to the theoretical value is marked with \* for the no-manipulation case.*

In contrast, the rejection rate improves *dramatically* just by using the spline kernel, and the rejection rate reaches around 90% in many cases. Plus, for all cases, the spline-type kernel dominates the triangular kernel. The power of the test with the spline kernel is relatively maintained when the sample size decreases, which is consistent with the efficiency analysis.

Lastly, we note that the performance of these kernels when the manipulation does not happen is quite similar and the rejection rate is close to the nominal level (see case (6)). These imply that the kernel choice does not deteriorate the size property.

All of these findings strongly support the use of the spline-type kernel instead of the triangular kernel. In the Online Appendix, we perform additional simulations using different DGPs and both estimated and theoretical fixed bandwidths, suggesting that our findings in this subsection are robust to such modifications.

### 3.4 Empirical Illustrations

In the Online Appendix, we report five empirical illustrations. We describe a summary of the results below: We first perform the manipulation test with the spline-type kernel for two empirical studies that are considered to be no manipulation in the literature (Lee et al., 2004 and Ludwig and Miller, 2007). For both cases, consistent results with the previous replications (Cattaneo et al., 2020; Cunningham, 2021) are confirmed. Second, we test the continuity of the running variable of the study by Ayres et al. (2021) and find a large discontinuity in contrast to their original finding. Third, we perform the discontinuity test using the data from Cattaneo et al. (2023a); see also Lindo et al. (2010). In that monograph, Cattaneo et al. (2023a, Section 4) reported that although the LPD-based test (with the triangular kernel) did not reject the continuity, there possibly be a density imbalance. Consistent with their remarks, the LPD-based test with the spline-type kernel rejects the continuity. Lastly, we test the density continuity of one of the running variables of the study by Eggers et al. (2021). While the original density estimation result produced wide confidence intervals and was thus perhaps too conservative, the LPD-based test with the spline-type kernel also does not reject continuity, suggesting the robustness of their design (at least with respect to density discontinuity). All of these results suggest a good performance of the LPD-based testing with the spline-type kernel.

## 4 Conclusion

We investigated how much and why kernel selection is important for boundary inference using the popular LPD estimator. Our main findings are that the kernel choice does matter for its variance properties and a well-chosen kernel function with non-compact support can largely improve the estimation and inference accuracy. As a prime example, we also studied the power property of the LPD-based discontinuity testing for RD designs and provided theoretical and numerical evidence that shows the performance greatly improves just by changing a kernel function to the spline-type kernel.

## A Kernel Selection for $\mathcal{K}$

We provide some details and justifications of the kernel functions in  $\mathcal{K}$ .

The uniform, triangular, and Epanechnikov kernels are included in the software packages prepared by Cattaneo et al. (2018, 2022) and thus should be considered. As all of these are compactly supported, the Gaussian and spline-type kernels are added to examine the behavior of non-compactly supported kernels. The Gaussian and Epanechnikov kernels would be two of the most popular kernel functions. The triangular kernel is the MSE-optimal in regression setting (Cheng et al., 1997), the uniform kernel is well used in practice due to its interpretability, and the spline-type kernel (Tsybakov, 2009, p.27; Silverman, 1984) has some optimality for a possibly discontinuous density in standard kernel estimation (Cline, 1990), though it is not popular.

We consider that comparing these kernels is informative. We highlight three points as to why the kernels in  $\mathcal{K}$  are important here. First, the triangular or Epanechnikov kernel can approximate many other compactly supported kernels. For example, biweight and triweight kernels have similar shapes to the triangular kernel, and in fact, we can confirm that their efficiency is almost equivalent to that of the triangular kernel. Second, considering a non-compactly supported kernel function whose tail decay is faster than the Gaussian kernel would not be necessary. As we have seen, the Gaussian kernel, which decays faster than the spline-type kernel, exhibits larger asymptotic variance and efficiency loss. Hence, we can induce that a faster decaying function would not produce a better property. In fact, one can confirm that  $K_e(u) = \exp(-|u|^3)/(2 \cdot \Gamma(4/3))$ , which decays faster, is less efficient than the Gaussian and spline-type kernels. Lastly, we would need not consider slower-decaying functions either. It should be natural to think about an algebraic decaying function for a candidate. Assume a simple example  $K_\rho(u) = 1/(1 + u^\rho) \cdot C_\rho$  with a scaling constant  $C_\rho$ . Then, we can easily find that small  $\rho$  (e.g.,  $\rho = 4$ ) leads to infinite (smaller-order) moments. When  $\rho$  is large, say  $\rho = 10$ , it can be confirmed that these are worse than the spline-type kernel. Besides, a much larger  $\rho$  leads to  $K_\rho(u) \simeq \mathbf{1}\{u^2 < 1\}/2$ , and thus, such a case can be approximated by the uniform kernel.

For these reasons, the comparison among  $\mathcal{K}$  will be informative enough to draw conclusions in a feasible way. (Although obtaining the optimal kernel may be appealing, it is known to be difficult even in the standard kernel density estimators (Müller (1991))) The asymptotic efficiency of the biweight, triweight,  $K_e$ , and  $K_\rho$  ( $\rho = 10$ ) is given in the Online Appendix.



## References

- Adams, A., Kluender, R., Mahoney, N., Wang, J., Wong, F., and Yin, W. (2022). The Impact of Financial Assistance Programs on Health Care Utilization: Evidence from Kaiser Permanente. *American Economic Review: Insights*, 4(3):389–407. [2](#)
- Ayres, A. B., Meng, K. C., and Plantinga, A. J. (2021). Do Environmental Markets Improve on Open Access? Evidence from California Groundwater Rights. *Journal of Political Economy*, 129(10):2817–2860. [2](#), [13](#), [S12](#), [S14](#)
- Britto, D. G. C., Pinotti, P., and Sampaio, B. (2022). The Effect of Job Loss and Unemployment Insurance on Crime in Brazil. *Econometrica*, 90(4):1393–1423. [2](#)
- Calonico, S., Cattaneo, M. D., and Farrell, M. H. (2018). On the Effect of Bias Estimation on Coverage Accuracy in Nonparametric Inference. *Journal of the American Statistical Association*, 113(522):767–779. [11](#), [S9](#)
- Calonico, S., Cattaneo, M. D., and Farrell, M. H. (2020). Optimal Bandwidth Choice for Robust Bias-Corrected Inference in Regression Discontinuity Designs. *The Econometrics Journal*, 23(2):192–210. [11](#), [S9](#)
- Calonico, S., Cattaneo, M. D., and Farrell, M. H. (2022). Coverage Error Optimal Confidence Intervals for Local Polynomial Regression. *Bernoulli*, 28(4):2998–3022. [11](#), [S9](#)
- Calonico, S., Cattaneo, M. D., and Titiunik, R. (2014). Robust Nonparametric Confidence Intervals for Regression-Discontinuity Designs. *Econometrica*, 82(6):2295–2326. [11](#), [S9](#)
- Cattaneo, M. D., Idrobo, N., and Titiunik, R. (2023a). A Practical Introduction to Regression Discontinuity Designs: Extensions. [13](#), [S12](#), [S13](#), [S14](#)
- Cattaneo, M. D., Jansson, M., and Ma, X. (2018). Manipulation Testing Based on Density Discontinuity. *The Stata Journal*, 18(1):234–261. [2](#), [12](#), [14](#), [S14](#), [S15](#), [S16](#)
- Cattaneo, M. D., Jansson, M., and Ma, X. (2020). Simple Local Polynomial Density Estimators. *Journal of the American Statistical Association*, 115(531):1449–1455. [2](#), [3](#), [4](#), [5](#), [6](#), [10](#), [11](#), [13](#), [S1](#), [S2](#), [S3](#), [S8](#), [S9](#), [S10](#), [S11](#), [S14](#), [S15](#)
- Cattaneo, M. D., Jansson, M., and Ma, X. (2021). Local Regression Distribution Estimators. *Journal of Econometrics*, forthcoming. [S10](#)
- Cattaneo, M. D., Jansson, M., and Ma, X. (2022). lpdensity: Local Polynomial Density Estimation and Inference. *Journal of Statistical Software*, 101(1):1–25. [14](#)
- Cattaneo, M. D., Keele, L., and Titiunik, R. (2023b). A Guide to Regression Discontinuity Designs in Medical Applications. *Statistics in Medicine*, 42(24):4484–4513. [2](#)
- Cattaneo, M. D. and Titiunik, R. (2022). Regression Discontinuity Designs. *Annual Review of Economics*, 14(1):821–851. [2](#)



- Chen, W.-L., Lin, M.-J., and Yang, T.-T. (2023). Curriculum and National Identity: Evidence from the 1997 Curriculum Reform in Taiwan. *Journal of Development Economics*, 163:103078. [2](#)
- Cheng, M.-Y., Fan, J., and Marron, J. S. (1997). On Automatic Boundary Corrections. *The Annals of Statistics*, 25(4):1691 – 1708. [14](#)
- Cline, D. B. H. (1990). Optimal Kernel Estimation of Densities. *Annals of the Institute of Statistical Mathematics*, 42:287–303. [14](#)
- Collin, M. and Talbot, T. (2023). Are Age-of-Marriage Laws Enforced? Evidence from Developing Countries. *Journal of Development Economics*, 160:102950. [2](#)
- Connolly, M. and Haeck, C. (2022). Nonlinear Class Size Effects on Cognitive and Noncognitive Development of Young Children. *Journal of Labor Economics*, 40(S1):S341–S382. [2](#)
- Cunningham, S. (2021). *Causal Inference: The Mixtape*. Yale University Press. [13](#), [S10](#), [S11](#), [S14](#)
- Dasgupta, U., Mani, S., Sharma, S., and Singhal, S. (2022). Effects of Peers and Rank on Cognition, Preferences, and Personality. *The Review of Economics and Statistics*, 104(3):587–601. [2](#)
- David, H. A. and Nagaraja, H. N. (2004). *Order Statistics*. John Wiley & Sons. [S5](#)
- DiNardo, J., Fortin, N. M., and Lemieux, T. (1996). Labor Market Institutions and the Distribution of Wages, 1973-1992: A Semiparametric Approach. *Econometrica*, 64(5):1001–1044. [2](#)
- Eggers, A. C., Ellison, M., and Lee, S. S. (2021). The Economic Impact of Recession Announcements. *Journal of Monetary Economics*, 120:40–52. [2](#), [13](#), [S13](#), [S14](#)
- Fan, J. and Gijbels, I. (1996). *Local Polynomial Modelling and Its Applications*. Chapman & Hall/CRC. [5](#), [S3](#)
- Gasser, T., Müller, H.-G., and Mammitzsch, V. (1985). Kernels for Nonparametric Curve Estimation. *Journal of the Royal Statistical Society: Series B (Methodological)*, 47(2):238–252. [6](#), [7](#)
- Gorrín, J., Morales-Arilla, J., and Ricca, B. (2023). Export Side Effects of Wars on Organized Crime: The Case of Mexico. *Journal of International Economics*, 144:103775. [2](#)
- Granovsky, B. L. and Müller, H.-G. (1991). Optimizing Kernel Methods: A Unifying Variational Principle. *International Statistical Review/Revue Internationale de Statistique*, pages 373–388. [7](#)
- Hall, P. (1992). Effect of Bias Estimation on Coverage Accuracy of Bootstrap Confidence Intervals for a Probability Density. *The Annals of Statistics*, pages 675–694. [S9](#)

- Hansen, B. E. (2022). *Econometrics*. Princeton University Press. 8
- He, G., Wang, S., and Zhang, B. (2020). Watering Down Environmental Regulation in China. *The Quarterly Journal of Economics*, 135(4):2135–2185. 2
- Kapoor, S., Oosterveen, M., and Webbink, D. (2021). The Price of Forced Attendance. *Journal of Applied Econometrics*, 36(2):209–227. 2
- Khanna, G. (2023). Large-Scale Education Reform in General Equilibrium: Regression Discontinuity Evidence from India. *Journal of Political Economy*, 131(2):549–591. 2
- Kinal, T. W. (1980). The Existence of Moments of k-Class Estimators. *Econometrica*, 48(1):241–249. 8
- Kosec, K. and Mo, C. H. (2023). Does Relative Deprivation Condition the Effects of Social Protection Programs on Political Support? Experimental Evidence from Pakistan. *American Journal of Political Science*. 2
- Lee, D. S., Moretti, E., and Butler, M. J. (2004). Do Voters Affect or Elect Policies? Evidence from the U. S. House. *The Quarterly Journal of Economics*, 119(3):807–859. 13, S10, S11, S14
- Lindo, J. M., Sanders, N. J., and Oreopoulos, P. (2010). Ability, Gender, and Performance Standards: Evidence from Academic Probation. *American Economic Journal: Applied Economics*, 2(2):95–117. 13, S12
- Ludwig, J. and Miller, D. L. (2007). Does Head Start Improve Children’s Life Chances? Evidence from a Regression Discontinuity Design. *The Quarterly Journal of Economics*, 122(1):159–208. 13, S10, S11, S14
- Ma, J. and Yu, Z. (2020). Coverage Optimal Empirical Likelihood Inference for Regression Discontinuity Design. *arXiv preprint arXiv:2008.09263*. S9
- Müller, H.-G. (1991). Smooth Optimum Kernel Estimators Near Endpoints. *Biometrika*, 78(3):521–530. 7, 14
- Nishiyama, Y. and Robinson, P. M. (2005). The Bootstrap and the Edgeworth Correction for Semiparametric Averaged Derivatives. *Econometrica*, 73(3):903–948. S9
- Seifert, B. and Gasser, T. (1996). Finite-Sample Variance of Local Polynomials: Analysis and Solutions. *Journal of the American Statistical Association*, 91(433):267–275. 3, 9, S6
- Silverman, B. W. (1984). Spline Smoothing: The Equivalent Variable Kernel Method. *The Annals of Statistics*, 12(3):898 – 916. 14
- Tsybakov, A. B. (2009). *Introduction to Nonparametric Estimation*. Springer New York. 14

# Online Appendix for “Kernel Choice Matters for Boundary Inference using Local Polynomial Density: With Application to Manipulation Testing”

Shunsuke Imai<sup>#</sup> and Yuta Okamoto<sup>#</sup>

<sup>#</sup>Graduate School of Economics, Kyoto University

January 30, 2024

## S1 Proofs

### S1.1 Notations and Setting

Let  $\mathcal{X} := (-\infty, x_R) \subseteq \mathbb{R}$  be the data domain. We are given independent and identically distributed samples  $X_{1:n} := (X_1, \dots, X_n)$  defined on  $\mathcal{X}$  with unknown distribution  $F$  and density  $f$ . The LPD estimator of Cattaneo et al. (2020) at a evaluation point  $x \in \mathcal{X}$  is given by

$$\hat{f}(x) := \mathbf{e}'_1 \hat{\boldsymbol{\beta}}(x),$$

$$\hat{\boldsymbol{\beta}}(x) := \arg \min_{\boldsymbol{\beta} \in \mathbb{R}^{p+1}} \sum_{i=1}^n \left\{ \hat{F}(X_i) - \mathbf{r}_p(X_i - x)' \boldsymbol{\beta} \right\}^2 \frac{1}{h} K\left(\frac{X_i - x}{h}\right),$$

where  $p$  is a positive integer such that  $p \geq 1$ ,  $\mathbf{e}_1$  is  $p + 1$  dimensional vector whose second element is 1 and the others are 0,  $\hat{F}(x) := n^{-1} \sum_{i=1}^n \mathbf{1}\{X_i \leq x\}$ ,  $\mathbf{r}_p(u) := (1, u, u^2, \dots, u^p)'$ ,  $K(\cdot)$  is a non-nnegative, symmetric kernel function such that  $\int K(u) du = 1$ , and  $h$  is a bandwidth such that  $h \rightarrow 0$  and  $nh \rightarrow \infty$ .

For notational simplicity, we write

$$u_{i,h} := \frac{X_i - x}{h}, \quad K_{i,h} := K(u_{i,h}), \quad \mathbf{K}_h := \text{diag}[K_{1,h}, \dots, K_{n,h}],$$

$$\mathbf{X}_h := [u_{i,h}^j]_{1 \leq i \leq n, 0 \leq j \leq p}, \quad \mathbf{H} := \text{diag}[1, h, \dots, h^p].$$

In addition, we define

$$\tilde{\mathbf{S}}_{(p,h,x)} := \frac{1}{nh} \mathbf{X}'_h \mathbf{K}_h \mathbf{X}_h = \frac{1}{nh} \sum_{i=1}^n \mathbf{r}_p(u_{i,h}) \mathbf{r}_p(u_{i,h})' K_{i,h},$$

$$\mathbf{S}_{(p,x)} := \int_{-\infty}^{(x_R - x)/h} \mathbf{r}_p(u) \mathbf{r}_p(u)' K(u) du.$$

For the analysis of the boundary point  $x_R$ , we introduce

$$\mathbf{A}_{p,K} = \int_{-\infty}^0 \mathbf{r}_p(u) \mathbf{r}_p(u)' K(u) du.$$

Note that  $\mathbf{S}_{(p,x_R)} = \mathbf{A}_{p,K}$ . Finally, for the finite sample analysis below, we define

$$\begin{aligned}\hat{\mathbf{F}} &:= (\hat{F}(X_1), \dots, \hat{F}(X_n))', \\ \tilde{\mathbf{\Omega}}_{(p,h,K)} &:= \frac{1}{h} \mathbf{X}'_h \mathbf{K}_h = \frac{1}{h} [K_{1,h} \mathbf{r}_p(u_{1,h}) \quad \dots \quad K_{n,h} \mathbf{r}_p(u_{n,h})].\end{aligned}$$

## S1.2 Derivation of the Equivalent Kernel

LPD has the following closed form:

$$\hat{f}(x) = \mathbf{e}'_1 \mathbf{H}^{-1} \tilde{\mathbf{S}}_{(p,h,x)}^{-1} \frac{1}{nh} \sum_{i=1}^n \mathbf{r}_p(u_{i,h}) K(u_{i,h}) \hat{F}(X_i).$$

Under the assumption of (i)  $h \rightarrow 0$  and  $nh \rightarrow \infty$  as  $n \rightarrow \infty$ , (ii)  $K(\cdot)$  is a non-negative, symmetric kernel function such that  $\int K(u) du = 1$  and (iii) the existence of the density function, we derive the equivalent kernel.

From Lemma 1 of Supplemental Appendix of [Cattaneo et al. \(2020\)](#) and the continuous mapping theorem, it follows that

$$\tilde{\mathbf{S}}_{(p,h,x)}^{-1} = \frac{1}{f(x)} \mathbf{S}_{(p,x)}^{-1} + o_p(1). \quad (\text{S1})$$

In addition, from a simple algebra, we can see that

$$\begin{aligned}& \frac{1}{nh} \sum_{i=1}^n \mathbf{r}_p(u_{i,h}) K(u_{i,h}) \hat{F}(X_i) \\ &= \int_{-\infty}^{(x_R-x)/h} \mathbf{r}_p(u) K(u) \hat{F}(x+uh) f(x+uh) du \\ & \quad + \frac{1}{nh} \sum_{i=1}^n \mathbf{r}_p(u_{i,h}) K(u_{i,h}) \left\{ \hat{F}(X_i) - F(X_i) \right\} \\ & \quad - \int_{-\infty}^{(x_R-x)/h} \mathbf{r}_p(u) K(u) \left\{ \hat{F}(x+uh) - F(x+uh) \right\} f(x+uh) du \\ & \quad + \frac{1}{nh} \sum_{i=1}^n \mathbf{r}_p(u_{i,h}) K(u_{i,h}) F(X_i) - \int_{-\infty}^{(x_R-x)/h} \mathbf{r}_p(u) K(u) F(x+uh) f(x+uh) du \\ &= \int_{-\infty}^{(x_R-x)/h} \mathbf{r}_p(u) K(u) \hat{F}(x+uh) f(x+uh) du \\ & \quad + \frac{1}{n^2 h} \sum_{i=1}^n \mathbf{r}_p(u_{i,h}) K(u_{i,h}) (1 - F(X_i)) \\ & \quad + \frac{1}{n^2 h} \sum_{i \neq j} \left\{ \mathbf{r}_p(u_{i,h}) \left( \mathbf{1}[X_j \leq X_i] - F(X_i) \right) K(u_{i,h}) \right. \\ & \quad \left. - \mathbb{E} \left[ \mathbf{r}_p(u_{i,h}) \left( \mathbf{1}[X_j \leq X_i] - F(X_i) \right) K(u_{i,h}) \mid X_j \right] \right\}\end{aligned}$$

$$\begin{aligned}
& + \frac{1}{nh} \sum_{i=1}^n \mathbf{r}_p(u_{i,h}) K(u_{i,h}) F(X_i) - \int_{-\infty}^{(x_R-x)/h} \mathbf{r}_p(u) K(u) F(x+uh) f(x+uh) du \quad (\text{S2}) \\
& = \int_{-\infty}^{(x_R-x)/h} \mathbf{r}_p(u) K(u) \hat{F}(x+uh) f(x+uh) du + \hat{\mathbf{B}}_{\text{LI}} + \hat{\mathbf{R}} + \hat{\mathbf{W}},
\end{aligned}$$

where  $\hat{\mathbf{B}}_{\text{LI}}$ ,  $\hat{\mathbf{R}}$  and  $\hat{\mathbf{W}}$  are the second, the third and the final terms in (S2) respectively. Lemma 2 and 4 of Supplemental Appendix of Cattaneo et al. (2020) state that  $\hat{\mathbf{B}}_{\text{LI}} = o_p(1)$  and  $\hat{\mathbf{R}} = o_p(1)$ . The convergence of  $\hat{\mathbf{W}}$  is obvious from the law of large numbers. So it holds that

$$\begin{aligned}
& \frac{1}{n} \sum_{i=1}^n \mathbf{r}_p(u_{i,h}) K(u_{i,h}) \hat{F}(X_i) \\
& = \int_{-\infty}^{(x_R-x)/h} \mathbf{r}_p(u) K(u) \hat{F}(x+uh) f(x+uh) du + o_p(1). \quad (\text{S3})
\end{aligned}$$

Since  $\mathbf{e}'_1 \mathbf{H}^{-1} = \frac{1}{h} \mathbf{e}'_1$ , (S1) and (S3) imply that

$$\begin{aligned}
\hat{f}(x) & = \frac{1}{h} \mathbf{e}'_1 \left\{ \frac{1}{f(x)} \mathbf{S}_{(p,x)}^{-1} \right\} \int_{-\infty}^{(x_R-x)/h} \mathbf{r}_p(u) K(u) \hat{F}(x+uh) f(x+uh) du + o_p(1) \\
& = \frac{1}{nh} \sum_{i=1}^n \int_{-\infty}^{(x_R-x)/h} \mathbf{e}'_1 \mathbf{S}_{(p,x)}^{-1} \mathbf{r}_p(u) K(u) \mathbf{1}\{u_{i,h} \leq u\} du + o_p(1).
\end{aligned}$$

That is, the equivalent kernel  $K^*$  is given by

$$K^*(v) = \int_{-\infty}^{(x_R-x)/h} \mathbf{e}'_1 \mathbf{S}_{(p,x)}^{-1} \mathbf{r}_p(u) K(u) \mathbf{1}\{v \leq u\} du.$$

### S1.3 Omitted Proofs

**Proof of Proposition 1.** As  $\text{supp}(K_{p,K}^*) = \text{supp}(K) \cap (-\infty, 0]$  and  $K_{p,K}^*(0) = 0$  are obvious, we only show the last part. Notice that  $\mathcal{K}(z) := \mathbf{e}'_1 \mathbf{A}_{p,K}^{-1} \mathbf{r}_p(z) K(z)$  is the usual equivalent kernel of local polynomial fitting for estimating the first derivative of regression function (Fan and Gijbels, 1996, p.70;  $K_{\nu,c}^*$  with  $\nu = 1, c = 0$  in their notation). Therefore,  $\mathcal{K}$  satisfies

$$\int_{-\infty}^0 z^j \mathcal{K}(z) dz = \delta_{1,j} \quad (0 \leq j \leq p), \quad (\text{S4})$$

where  $\delta_{1,j}$  takes 1 if  $j = 1$  and 0 otherwise. Since, from the standard property of the integration and (S4) with  $j = 0$ ,

$$\int_{-\infty}^0 \mathcal{K}(z) \mathbf{1}\{u \leq z\} dz = \int_{-\infty}^0 \mathcal{K}(z) dz - \int_{-\infty}^u \mathcal{K}(z) dz = - \int_{-\infty}^0 \mathcal{K}(z) \mathbf{1}\{z \leq u\} dz,$$

it holds that

$$\begin{aligned} \int_{-\infty}^0 u^j K_{p,K}^*(u) du &= \int_{-\infty}^0 u^j \left\{ \int_{-\infty}^0 \mathcal{K}(z) \mathbf{1}\{u \leq z\} dz \right\} du \\ &= \int_{-\infty}^0 u^j \left\{ - \int_{-\infty}^0 \mathcal{K}(z) \mathbf{1}\{u \geq z\} dz \right\} du. \end{aligned} \quad (\text{S5})$$

In addition, by a simple evaluation, we can see that

$$\int_{-\infty}^0 \int_{-\infty}^0 \left| u^j \mathcal{K}(z) \mathbf{1}\{u \geq z\} \right| du dz \leq \frac{1}{j+1} \int_{-\infty}^0 \sum_{k=0}^p |a_k| |z|^{k+j+1} K(z) dz,$$

so, since  $\int_0^\infty u^{2p} K(u) du < \infty$ , the order of the integration in (S5) is exchangeable. Therefore

$$\begin{aligned} \int_{-\infty}^0 u^j K_{p,K}^*(u) du &= - \int_{-\infty}^0 \mathcal{K}(z) \int_z^0 u^j du dz \\ &= \frac{1}{j+1} \int_{-\infty}^0 \mathcal{K}(z) z^{j+1} dz = \frac{\delta_{0,j}}{j+1} \quad (0 \leq j \leq p-1). \end{aligned}$$

□

**Proof of Theorem 1.** In the proof of Theorem 1,  $f(x)$  is supported by a bounded region  $\mathcal{S} := [x_L, x_R)$  by Assumption 2. Put  $\mathbb{E}_2[\cdot] = \mathbb{E}[\cdot | n_0 = 2]$ . Below, we show the statement by proving

$$\mathbb{E}_2 \left[ \hat{f}(x_R)^2 \right] \mathbb{P}[n_0 = 2] = \infty,$$

because  $\mathbb{E} \left[ \hat{f}(x_R)^2 \right] \geq \mathbb{E}_2 \left[ \hat{f}(x_R)^2 \right] \mathbb{P}[n_0 = 2]$ . Let  $X_{(1)}, X_{(2)}, \dots, X_{(n-1)}, X_{(n)}$  be ordered observations. Now, since we use a compactly supported kernel, supposing the standard weighted least square regression with two data points, we have

$$\mathbb{E}_2 \left[ \hat{f}(x_R)^2 \right] = \mathbb{E}_2 \left[ \left( \frac{\hat{F}(X_{(n)}) - \hat{F}(X_{(n-1)})}{(X_{(n)} - x_R) - (X_{(n-1)} - x_R)} \right)^2 \right], \quad (\text{S6})$$

where we utilize the fact that the coefficient can be considered as the ‘‘slope’’ of the straight line through two data. Note that this holds regardless of the kernel function as long as Assumption 1 is satisfied. Then, noticing that  $\hat{F}(X_{(n)}) = 1$  and  $\hat{F}(X_{(n-1)}) = 1 - 1/n$  from the definition of the empirical distribution function, we have

$$\begin{aligned} \mathbb{E}_2 \left[ \hat{f}(x_R)^2 \right] &= \mathbb{E}_2 \left[ \frac{\{1 - (1 - 1/n)\}^2}{\{X_{(n)} - X_{(n-1)}\}^2} \right] \\ &\geq \mathbb{E}_2 \left[ \frac{(1/n)^2}{\{x_R - X_{(n-1)}\}^2} \right]. \end{aligned} \quad (\text{S7})$$

By the way, it follows from the definition of the conditional expectation that

$$\mathbb{E}_2 \left[ \frac{(1/n)^2}{\{x_R - X_{(n-1)}\}^2} \right] = \frac{1}{n^2} \times \frac{1}{P_1} \int_{\mathcal{S}} \frac{1}{(x_R - z)^2} \tilde{\mathbb{P}}(z) dz, \quad (\text{S8})$$

where  $P_1 = \mathbb{P}[n_0 = 2]$  and  $\tilde{\mathbb{P}}(z)$  is defined by

$$\tilde{\mathbb{P}}(z) dz = \mathbb{P} [n_0 = 2 \text{ and } X_{(n-1)} \in [z - dz/2, z + dz/2]].$$

Since the joint density of all  $n$  ordered statics is  $n!f(x_1)f(x_2)\cdots f(x_n)$  with  $x_1 < x_2 < \cdots < x_n$  (David and Nagaraja, 2004, p.12), we have, with  $\tilde{f}(z) = f_X(z)1\{x_R - h \leq z\}$ ,

$$\begin{aligned} \tilde{\mathbb{P}}(z) dz &= dz \int_z^{x_R} \int_{x_L}^{x_R-h} \int_{x_L}^{x_{n-2}} \cdots \int_{x_L}^{x_3} \int_{x_L}^{x_2} n!f(x_1)\cdots f(x_{n-2})\tilde{f}(z)f(x_n) dx_1 \dots dx_{n-2} dx_n \\ &\geq dz \cdot n! \delta^{n-1} \tilde{f}(z) \int_z^{x_R} \int_{x_L}^{x_R-h} \int_{x_L}^{x_{n-2}} \cdots \int_{x_L}^{x_3} \int_{x_L}^{x_2} 1 dx_1 \dots dx_{n-2} dx_n \\ &= dz \cdot n! \delta^{n-1} \tilde{f}(z) C(n, h, x_L, x_R) \int_z^{x_R} 1 dx_n \\ &= dz \cdot n! \delta^{n-1} \tilde{f}(z) C(n, h, x_L, x_R) \cdot (x_R - z), \end{aligned}$$

where the inequality follows from Assumption 2, and  $C(n, h, x_L, x_R)$  is some constant depending on  $n, h, x_L$ , and  $x_R$ . This implies, letting  $\int_{x_R-h}^{x_R}$  denotes  $\lim_{x \rightarrow x_R} \int_{x_R-h}^x$ , that the conditional expectation (S8) is bounded as

$$\begin{aligned} \mathbb{E}_2 \left[ \frac{(1/n)^2}{\{2(x_R - X_{(n-1)})\}^2} \right] &= \frac{n!}{P_1 n^2} \int_{\mathcal{S}} \frac{1}{(x_R - z)^2} \tilde{\mathbb{P}}(z) dz \\ &\geq \frac{n!}{P_1 n^2} \delta^{n-1} C(n, h, x_L, x_R) \int_{x_L}^{x_R} \frac{1}{(x_R - z)} \tilde{f}_X(z) dz \\ &= \frac{n!}{P_1 n^2} \delta^{n-1} C(n, h, x_L, x_R) \int_{x_R-h}^{x_R} \frac{1}{(x_R - z)} f_X(z) dz \\ &\geq \frac{n!}{P_1 n^2} \delta^n C(n, h, x_L, x_R) \int_{x_R-h}^{x_R} \frac{1}{(x_R - z)} dz. \end{aligned}$$

Now we have that

$$\begin{aligned} \mathbb{E} \left[ \hat{f}(x_R)^2 \right] &\geq \mathbb{E}_2 \left[ \hat{f}(x_R)^2 \right] \mathbb{P} [n_0 = 2] \\ &\geq \frac{n! \delta^n C(n, h, x_L, x_R)}{n^2} \int_{x_R-h}^{x_R} \frac{1}{x_R - z} dz \\ &= \infty. \end{aligned}$$

Proof completes.  $\square$

We here explain how their proof and ours relate to each other. Write regression function by  $r(x)$ , its estimator by  $\hat{r}(x)$ , and density of the regressor by  $f(x)$ . They assume the error satisfies  $\mathbb{V}[\varepsilon_i] = \sigma^2$ , and  $[x_L, x_R] = [0, 1)$ . We write some bounded constants by  $C_j$ .



Utilizing the homoskedasticity assumption and the law of total variance repeatedly, they show that

$$\mathbb{V}[\hat{r}(x_R)] \geq C_1 \times \mathbb{V}_{U,r \equiv 0, f \equiv 1}[\hat{r}(x)|n_0 = 2],$$

where  $\mathbb{V}_{U,r \equiv 0, f \equiv 1}$  is the variance when using the uniform kernel,  $r(x) \equiv 0$ , and  $f(x) \equiv 1$ . Although [Seifert and Gasser \(1996\)](#) immediately conclude that the last term equals infinity, an important point would be in the omitted part, as it will show what happens and clarify what the connection is. Now, note that we can write

$$\mathbb{V}_{U,r \equiv 0, f \equiv 1}[\hat{r}(x_R) | n_0 = 2] = \mathbb{E}_{2,r \equiv 0, f \equiv 1} \left[ \left( \frac{Y_{(n)} - Y_{(n-1)}}{X_{(n)} - X_{(n-1)}} \right)^2 \right] - C_2 \quad (\text{S9})$$

$$= \mathbb{E}_{2,r \equiv 0, f \equiv 1} \left[ \left( \frac{\varepsilon_{(n)} - \varepsilon_{(n-1)}}{X_{(n)} - X_{(n-1)}} \right)^2 \right] - C_2 = \mathbb{E}_{2,r \equiv 0, f \equiv 1} \left[ \frac{2\sigma^2}{(X_{(n)} - X_{(n-1)})^2} \right] - C_2, \quad (\text{S10})$$

where  $(Y_{(n)}, \varepsilon_{(n)})$  is  $(Y, \varepsilon)$  that corresponds to  $X_{(n)}$ . We can show this is infinite by following similar steps as we take in our proof since (S10) is essentially the same as (S7). Now we can see that the LPD and the local linear regression share a similar structure through (S7) and (S10), which are a direct consequence of (S6) and (S9). This fact suggests the fundamental factor for the variance property is the same: Roughly speaking, when the local sample size is small relative to the polynomial degree, the local polynomial overfits the data, and in such a case, the estimate or the slope can take an arbitrarily large value with a certain probability, since the data point can be located close enough.

**Corollary S1.** *Under the same assumption for Theorem 1, the local polynomial density estimator  $\hat{f}(x_R)$  of degree  $p = 2$  does not have a second moment.* ♣

**Proof of Corollary S1.** We write  $\mathbb{E}_{3,\circ}[\cdot] = \mathbb{E}[\cdot | n_0 = 3, \circ]$ . Based on a similar idea to Theorem 1, supposing a quadratic polynomial regression with three data points, a straightforward calculation yields

$$\begin{aligned} & \mathbb{E}_3 \left[ \hat{f}(x_R)^2 \right] \\ &= \mathbb{E}_3 \left[ \left( \frac{X_{(n)}^2 - 2X_{(n-1)}^2 + X_{(n-2)}^2 - 2x_R (X_{(n)} - 2X_{(n-1)} + X_{(n-2)})}{n (X_{(n)} - X_{(n-1)}) (X_{(n)} - X_{(n-2)}) (X_{(n-1)} - X_{(n-2)})} \right)^2 \right] \\ &= \mathbb{E}_3 \left[ \left( \frac{2x_R - (X_{(n-1)} + X_{(n-2)})}{n (X_{(n)} - X_{(n-2)}) (X_{(n)} - X_{(n-1)})} - \frac{2x_R - (X_{(n)} + X_{(n-1)})}{n (X_{(n)} - X_{(n-2)}) (X_{(n-1)} - X_{(n-2)})} \right)^2 \right]. \end{aligned}$$

Now let  $\mathcal{E}$  denote the event  $\{X_{(n-2)} \in [x_R - h, x_R - 2h/3) \text{ and } X_{(n-1)}, X_{(n)} \in [x_R - h/3, x_R)\}$ . Note that  $\mathbb{P}[n_0 = 3, \mathcal{E}] > 0$ , and under  $\mathcal{E}$ , the first term in the bracket is larger than the second and both are positive. Then we have

$$\mathbb{E}_{3,\mathcal{E}} \left[ \left( \frac{2x_R - (X_{(n-1)} + X_{(n-2)})}{n (X_{(n)} - X_{(n-2)}) (X_{(n)} - X_{(n-1)})} - \frac{2x_R - (X_{(n)} + X_{(n-1)})}{n (X_{(n)} - X_{(n-2)}) (X_{(n-1)} - X_{(n-2)})} \right)^2 \right]$$

$$\begin{aligned}
&\geq \mathbb{E}_{3,\varepsilon} \left[ \left( \frac{2x_R - (X_{(n-1)} + X_{(n-2)})}{nh(X_{(n)} - X_{(n-1)})} - \frac{2x_R - (X_{(n)} + X_{(n-1)})}{nh(X_{(n-1)} - X_{(n-2)})} \right)^2 \right] \\
&\geq \mathbb{E}_{3,\varepsilon} \left[ \left( \frac{x_R - X_{(n-2)}}{nh(X_{(n)} - X_{(n-1)})} - \frac{x_R - X_{(n)}}{nh(X_{(n-1)} - X_{(n-2)})} \right)^2 \right] \\
&\geq \mathbb{E}_{3,\varepsilon} \left[ \left( \frac{x_R - X_{(n-2)}}{nh(x_R - X_{(n-1)})} - \frac{h/3}{nh(h/3)} \right)^2 \right] \\
&\geq \mathbb{E}_{3,\varepsilon} \left[ \left( \frac{h/3}{nh(x_R - X_{(n-1)})} - \frac{1}{nh} \right)^2 \right].
\end{aligned}$$

The remainder is completely the same as before.  $\square$

**Proof of Theorem 1'.** With no loss of generality, we can set  $x_R = 0$  and  $x_L = -L$  with  $L > 0$ . The LPD estimator with polynomial order  $p = 1$  at the boundary point  $x_R = 0$  is given by

$$\hat{f}(0) = \frac{1}{nh} \mathbf{e}'_1 \tilde{\mathbf{S}}_{(1,h,0)}^{-1} \tilde{\mathbf{\Omega}}_{(1,h,0)} \hat{\mathbf{F}}.$$

To prove Theorem 1', we bound the second moment of this estimator without relying on asymptotics:

$$\mathbb{E} \left[ \hat{f}^2(0) \right] = \mathbb{E} \left[ \left( \frac{1}{nh} \mathbf{e}'_1 \tilde{\mathbf{S}}_{(1,h,0)}^{-1} \tilde{\mathbf{\Omega}}_{(1,h,0)} \hat{\mathbf{F}} \right)^2 \right]$$

First, we rewrite  $\tilde{\mathbf{S}}_{(1,h,0)}^{-1}$  as  $\tilde{\mathbf{S}}_{(1,h,0)}^{-1} = |\tilde{\mathbf{S}}_{(1,h,0)}|^{-1} \tilde{\mathbf{M}}_{(1,h,0)}$  with

$$|\tilde{\mathbf{S}}_{(1,h,0)}| := \det(\tilde{\mathbf{S}}_{(1,h,0)}), \quad \tilde{\mathbf{M}}_{(1,h,0)} := \begin{bmatrix} \frac{1}{nh} \sum_{i=1}^n u_{i,h}^2 K_{i,h} & -\frac{1}{nh} \sum_{i=1}^n u_{i,h} K_{i,h} \\ -\frac{1}{nh} \sum_{i=1}^n u_{i,h} K_{i,h} & \frac{1}{nh} \sum_{i=1}^n K_{i,h} \end{bmatrix}.$$

Using this notation, the second moment can be represented as:

$$\mathbb{E} \left[ \hat{f}^2(0) \right] = \mathbb{E} \left[ \left( \frac{1}{nh} \mathbf{e}'_1 |\tilde{\mathbf{S}}_{(1,h,0)}|^{-1} \tilde{\mathbf{M}}_{(1,h,0)} \tilde{\mathbf{\Omega}}_{(1,h,0)} \hat{\mathbf{F}} \right)^2 \right].$$

Next, we bound the inverse of the determinant and the "numerator" part separately. The determinant  $|\tilde{\mathbf{S}}_{(1,h,0)}|$  is bounded as

$$|\tilde{\mathbf{S}}_{(1,h,0)}| = \left( \frac{1}{nh} \sum_{i=1}^n K_{i,h} \right) \left( \frac{1}{nh} \sum_{i=1}^n u_{i,h}^2 K_{i,h} \right) - \left( \frac{1}{nh} \sum_{i=1}^n u_{i,h} K_{i,h} \right)^2$$

$$\begin{aligned}
&= \frac{1}{n^2 h^2} \sum_{i < j} K_{i,h} K_{j,h} (u_{i,h} - u_{j,h})^2 \\
&= \frac{1}{n^2 h^4} \sum_{i < j} K_{i,h} K_{j,h} (X_i - X_j)^2 \geq \frac{K^2(-L/h)}{n^2 h^4} (X_{(1)} - X_{(n)})^2.
\end{aligned}$$

In addition, we can bound the "numerator" component as

$$\begin{aligned}
&\frac{1}{nh} e'_1 \tilde{M}_{(1,h,0)} \tilde{\Omega}_{(1,h,0)} \hat{F} \\
&= \left( \frac{1}{nh^2} \sum_{i=1}^n u_{i,h} K_{i,h} \hat{F}(X_i) \right) \left( \frac{1}{nh} \sum_{i=1}^n K_{i,h} \right) - \left( \frac{1}{nh^2} \sum_{i=1}^n K_{i,h} \hat{F}(X_i) \right) \left( \frac{1}{nh} \sum_{i=1}^n u_{i,h} K_{i,h} \right) \\
&< \left( \frac{1}{nh^2} \sum_{i=1}^n K_{i,h} \hat{F}(X_i) \right) \left( \frac{1}{nh^2} \sum_{i=1}^n L K_{i,h} \right) \\
&< \frac{L}{h^4} K^2(0).
\end{aligned}$$

where the second inequality follows from  $-L/h \leq u_{i,h} \leq 0$  and the non-negativity of  $L$ ,  $h$ ,  $K_{i,h}$  and  $\hat{F}(X_i)$  and the final inequality follows from  $K_{i,h} \leq K(0)$  and  $\hat{F}(X_i) \leq 1$ . Similarly, we can show that

$$\frac{1}{nh} e'_1 \tilde{M}_{(1,h,0)} \tilde{\Omega}_{(1,h,0)} \hat{F} > - \left( \frac{L}{h^4} K^2(0) \right).$$

Therefore, we can see that

$$\mathbb{E} \left[ \hat{f}^2(0) \right] < \left( \frac{n^2 L K^2(0)}{K^2(-L/h)} \right)^2 \mathbb{E} \left[ \frac{1}{(X_{(1)} - X_{(n)})^4} \right].$$

Finally, using the same notations as those for the proof of Theorem 1, we can evaluate the expectation,

$$\begin{aligned}
&\mathbb{E} \left[ \frac{1}{(X_{(1)} - X_{(n)})^4} \right] \\
&= \int_{-L}^0 \int_{-L}^{x_n} \int_{-L}^{x_{n-1}} \cdots \int_{-L}^{x_3} \int_{-L}^{x_2} \frac{1}{(x_1 - x_n)^4} n! f(x_1) \cdots f(x_n) dx_1 dx_2 \cdots dx_{n-1} dx_n \\
&< n! \Delta^n \int_{-L}^0 \int_{-L}^{x_n} \int_{-L}^{x_{n-1}} \cdots \int_{-L}^{x_3} \int_{-L}^{x_2} \frac{1}{(x_1 - x_n)^4} dx_1 dx_2 \cdots dx_{n-1} dx_n.
\end{aligned}$$

We can show this is bounded by a constant that depends only on  $L$  and  $n$  by evaluating the integration above in order. (The requirement  $n \geq 7$  is used for this operation.)  $\square$

## S2 Technical Remarks

In this section, we provide detailed remarks on the test statistic  $T_3(h_2^{\text{MSE}})$ . First, we describe the idea behind  $T_3(h_2^{\text{MSE}})$  based on the argument in [Cattaneo et al. \(2020, p.1453\)](#). Next,

we discuss the refinement of  $T_3(h_2^{\text{MSE}})$  in view of the previous works on the local polynomial smoothing, which underscores the usefulness of our discussion on kernel selection in the main article.

## S2.1 Simple Robust Bias Correction

As noted in [Calonico et al. \(2014, Remark 7\)](#), the local polynomial estimator of order  $p + 1$  with a bandwidth  $h$  is equivalent to explicitly bias-corrected local polynomial estimator of order  $p$  constructed by using the bandwidth  $h$  for both estimator itself and bias estimator. Also, this fact implies that the variance of the estimator of order  $p + 1$  captures the uncertainty of the density estimation and bias estimation. So, the test statistic  $T_3(h_2^{\text{MSE}})$  may be considered a robustly bias-corrected test statistic. Based on this idea, [Cattaneo et al. \(2020\)](#) proposes to use it.

## S2.2 Higher-Order Refinement

We note the relation to the previous works on local polynomial smoothing. Recalling the poor testing performance we have seen in Section 1 (Figure 1a) and recent developments in local polynomial smoothing techniques, we can naturally suppose there are some possible directions for improving the accuracy of inference (in ways other than changing the kernel).

Given the results of [Calonico et al. \(2018\)](#), studentization by the fixed- $n$  variance estimator will be much preferable. In addition, it is also desirable to derive a type of optimal bandwidth for the inference by deriving a second-order Edgeworth expansion as in [Hall \(1992\)](#), [Nishiyama and Robinson \(2005\)](#), [Ma and Yu \(2020\)](#) and [Calonico et al. \(2018, 2020, 2022\)](#). However, the refinement attempts in these directions are challenging. As to the construction of the fixed- $n$  variance estimator of LPD, a non-trivial ingenuity seems to be required because the dependent variable (the empirical distribution function in the LPD case) depends on the whole sample  $X_{1:n}$ . Also, the derivation of the Edgeworth expansion is quite demanding and not an easy task.

Therefore, kernel selection would be one of the few viable options for refining the power of LPD-based manipulation testing. Besides, we can say this direction of refinement is quite natural in that the general theory described in Section 2 suggests that we can possibly enjoy a substantial efficiency gain just by changing the kernel function, which could lead to an improvement in the statistical power.

## S3 Asymptotic Efficiency

We report the full list of the asymptotic variance, efficiency, and  $\Theta_K$  for both boundary and interior points. See Table [S1](#).

### S3.1 Some By-Product Results for Interior Points

In this subsection, we briefly list some findings regarding the LPD estimation at interior points. In Table [S1](#), we compute  $\mathcal{V}_{2,K}$  and  $\mathcal{Q}_{2,K}$  for kernels in  $\mathcal{K}$ . Similarly to before, the

Kernel Function	Boundary							Interior		
	$\mathcal{V}_{1,K}$	$\mathcal{V}_{2,K}$	$\mathcal{V}_{3,K}$	$\mathcal{Q}_{1,K}$	$\mathcal{Q}_{2,K}$	$\mathcal{Q}_{3,K}$	$\Theta_K$	$\mathcal{V}_{2,K}$	$\mathcal{Q}_{2,K}$	$\Theta_K$
Triangular	1.37143 (5.49)	5.71429 (7.62)	14.026 (9.97)	1.06376 (1.06)	2.87329 (1.14)	5.9886 (1.21)	7.05261 (1.49)	0.742857 (4.75)	0.546447 (0.89)	1.06817 (1.18)
Uniform	1.2 (4.80)	5.48571 (7.31)	14.2857 (10.16)	1.12924 (1.13)	3.18161 (1.26)	6.83074 (1.38)	8.28544 (1.75)	0.6 (3.84)	0.541728 (0.89)	1.1286 (1.25)
Epanechnikov	1.34547 (5.38)	5.77201 (7.70)	14.4678 (10.29)	1.08683 (1.09)	2.99072 (1.18)	6.32592 (1.28)	7.49635 (1.58)	0.714286 (4.57)	0.544386 (0.89)	1.07259 (1.18)
Gaussian	0.483582 (1.93)	1.7485 (2.33)	3.80874 (2.71)	1.0408 (1.04)	2.73937 (1.08)	5.56648 (1.13)	5.96715 (1.26)	0.282095 (1.81)	0.563851 (0.92)	0.951499 (1.05)
Spline	0.25 (1.00)	0.75 (1.00)	1.40625 (1.00)	1 (1.00)	2.5244 (1.00)	4.93485 (1.00)	4.73325 (1.00)	0.15625 (1.00)	0.611968 (1.00)	0.906052 (1.00)
$K_3^e$	0.896426 (3.59)	3.49339 (4.66)	8.074 (5.74)	1.06619 (1.07)	2.87189 (1.14)	5.95326 (1.21)	6.63758 (1.40)	0.501077 (3.21)	0.552268 (0.90)	0.985737 (1.09)
$K_{10}^p$	0.967888 (3.87)	3.35494 (4.47)	5.87033 (4.17)	1.08989 (1.09)	2.93309 (1.16)	6.28559 (1.27)	5.1322 (1.08)	0.528657 (3.38)	0.551725 (0.90)	0.861236 (0.95)
Biweight	1.49636 (5.99)	6.18362 (8.24)	15.1082 (10.74)	1.07103 (1.07)	2.91176 (1.15)	6.10338 (1.24)	7.11421 (1.50)	0.815851 (5.22)	0.547571 (0.89)	1.04361 (1.15)
Triweight	1.63889 (6.56)	6.61057 (8.81)	15.8645 (11.28)	1.06306 (1.06)	2.86944 (1.14)	5.97919 (1.21)	6.8863 (1.45)	0.907034 (5.81)	0.550035 (0.90)	1.02584 (1.13)

**Table S1:** Full List of Asymptotic Efficiency

Gaussian and spline-type kernel achieves smaller variance, but the compactly supported kernels are better than these two in the MSE-efficiency sense. Among the five kernels, the uniform kernel is the best. This is consistent with [Cattaneo et al. \(2021\)](#), in which they found the equivalent kernel of the LPD with the uniform kernel was the Epanechnikov kernel, i.e., MSE optimal. Another interesting fact may be that the LPD with the Gaussian is equivalent to the KDE with the Gaussian kernel, which can be confirmed again by the equivalent kernel argument. We also compute  $\Theta_K$  at interior points. Importantly, the spline-type kernel is the best among  $\mathcal{K}$  and the efficiency gain is a certain degree, though not as large as at the boundary (in both absolute and relative terms). Therefore, when the main objective is inference, the use of the spline-type kernel will be preferred. For uniform inference, the kernel choice may be important. However, we note that  $K_{10}$  is more efficient than the spline kernel, and hence, investigation in this direction may perhaps be fruitful.

## S4 Empirical Illustrations

Below, we report several empirical examples. For all cases, the nominal level is 0.05. As a whole, we find that (i) the spline-type kernel produces a sharper confidence interval, and (ii) published work using RD analysis is often well-designed.

### S4.1 Lee, Moretti, Butler (2004); Ludwig and Miller (2007)

We first treat the studies by [Lee et al. \(2004\)](#) and [Ludwig and Miller \(2007\)](#). The continuity of the density of the running variable for these studies is tested in [Cunningham \(2021\)](#) and [Cattaneo et al. \(2020\)](#), respectively, and the discontinuity is not detected for both. We confirm if the previous results do not flip by using the [Cattaneo et al. \(2020\)](#)'s test with the

spline kernel, which was found to be recommendable in the main paper.

We first consider the work by [Lee et al. \(2004\)](#). The running variable is the vote share, and its density continuity was examined in [Cunningham \(2021, pp.310-311\)](#). We perform the [Cattaneo et al. \(2020\)](#)'s test with the triangular and spline kernel. The results are shown in Figure S1. Both do not reject the null and are consistent with [Cunningham \(2021\)](#)'s conclusion.

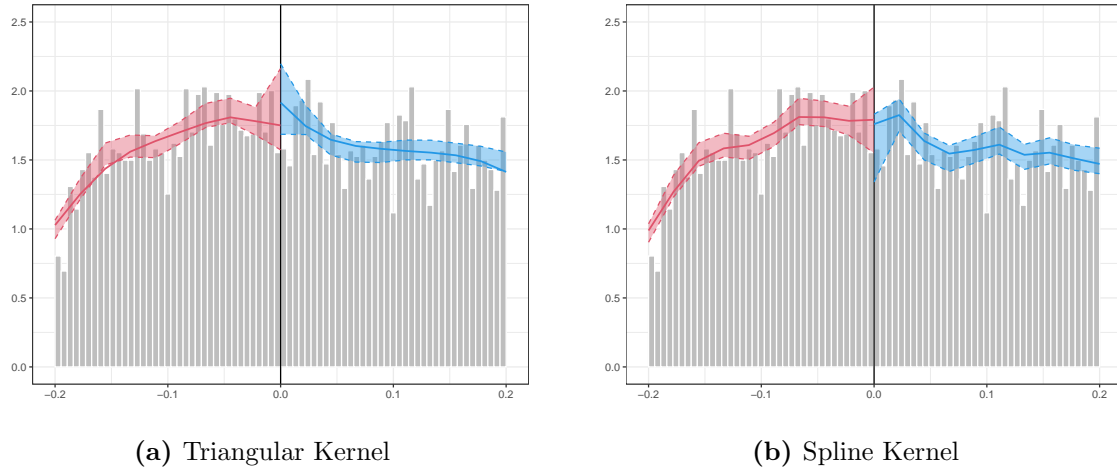


**Figure S1:** Density Test for [Lee et al. \(2004\)](#). *The cutoff point is normalized to 0*

Similarly, we do not detect the discontinuity for [Ludwig and Miller \(2007\)](#) based on the same analysis. See Figure S2. This is also consistent with [Cattaneo et al. \(2020\)](#)'s.

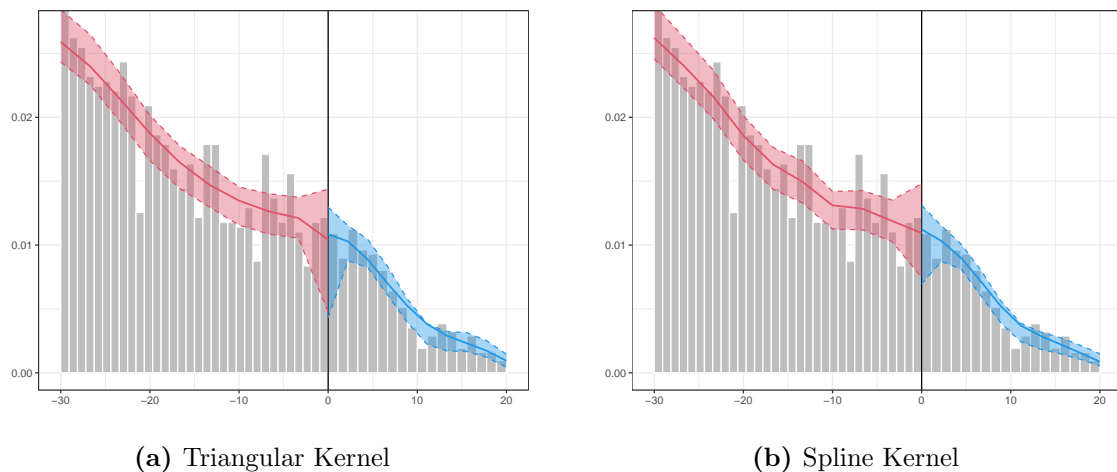


**Figure S2:** Density Test for [Ludwig and Miller \(2007\)](#). *The cutoff point is normalized to 0.*

Taken together, these results seem to suggest that the spline kernel would not be prone to overly reject the null and that the use of it is a recommended choice.

## S4.2 Ayres, Meng, and Plantinga (2021)

Ayres et al. (2021) investigated if and how much a groundwater market introduced in the 1990s to the Mojave Desert had generated net benefit, which is capitalized in land value. They used the distance from the spatial boundary as a running variable. In the paper, they performed the LPD-based manipulation testing. They reported they did not detect a discontinuity in the density using the LPD-based manipulation testing (Ayres et al., 2021, pp.2844-2845).

We reassess the continuity of the density of the running variable using the LPD-based test with the spline kernel. Figure S3b displays the estimated density with the spline kernel. It exhibits a large jump in the density of the running variable. Correspondingly, the  $p$ -value of the manipulation testing with the spline kernel is computed as  $6.76281 \times 10^{-110}$ . Therefore, the null hypothesis, or the continuity at the cutoff, is rejected.

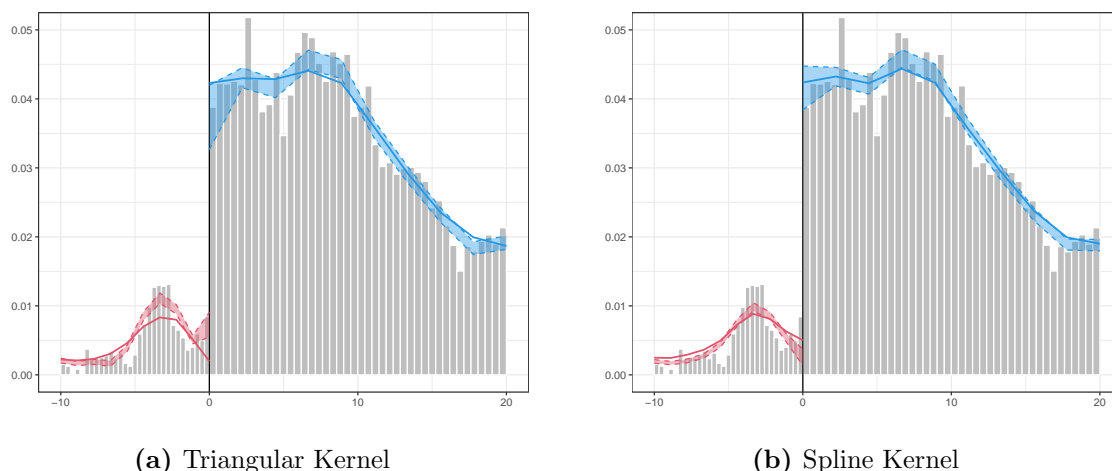


**Figure S3:** Density Test for Ayres et al. (2021)

As is evident from Figure S3a, we rejected the continuity even with the triangular kernel. The difference between Ayres et al. (2021)'s and our result may perhaps be due to the difference in software (they mainly used `Stata` while our analysis is produced using `R`), its version, or the chosen bandwidth.

## S4.3 Cattaneo, Idrobo, and Titiunik (2023)

Cattaneo et al. (2023a, Section 4)<sup>1</sup> re-analyzed the study by Lindo et al. (2010), who assessed the effect of academic probation on their future educational attainment, using a subset of the original data. Cattaneo et al. (2023a, Section 4.3) provides some observations that may suggest the imbalance in the density of the running variable (GPA) at the threshold, whereas they reported that the LPD-based manipulation testing failed to reject the continuity ( $p$ -value was 0.082).

---

<sup>1</sup>We accessed the latest manuscript on Matias D. Cattaneo's website: <https://cattaneo.princeton.edu/publications> (final access: December 24, 2023)



This may be due to the large variance derived from the triangular kernel. Thus, we perform the manipulation test using the spline-type kernel. As a result, the LPD-based test rejects the continuity ( $p$ -value was 0.020).

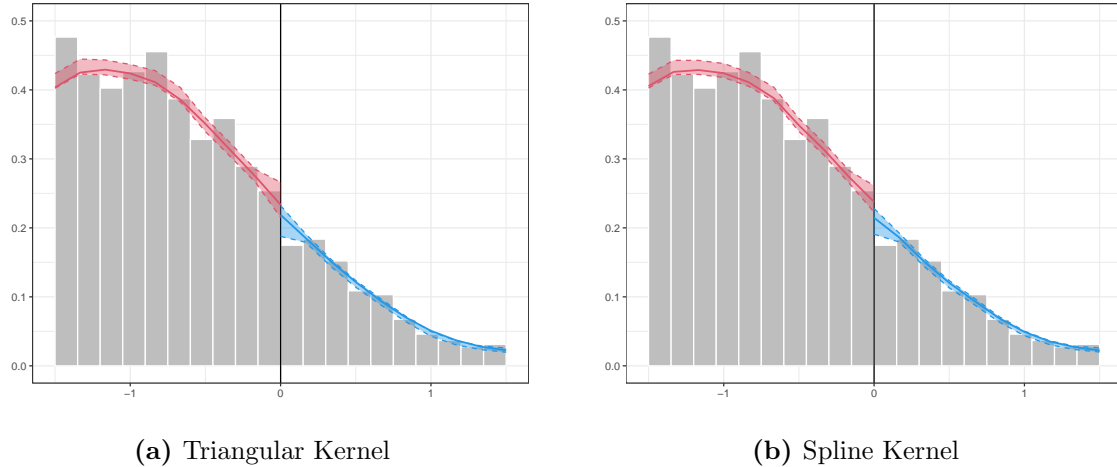


**Figure S4:** Density Test for [Cattaneo et al. \(2023a\)](#)

#### S4.4 Eggers, Ellison, and Lee (2021)

[Eggers et al. \(2021\)](#) investigated the macroeconomic impact of recession announcements. They performed the LPD-based discontinuity testing for their running variables (see their equation (1) and subsequent argument). While the continuity was not rejected, the reported figure shows very wide confidence intervals ([Eggers et al., 2021](#), Fig. 2, right panel).

To assess the robustness, we conduct the LPD-based manipulation testing with the spline-type kernel. As a result, [Figure S5b](#) shows much sharper confidence intervals and the test does not reject the continuity.

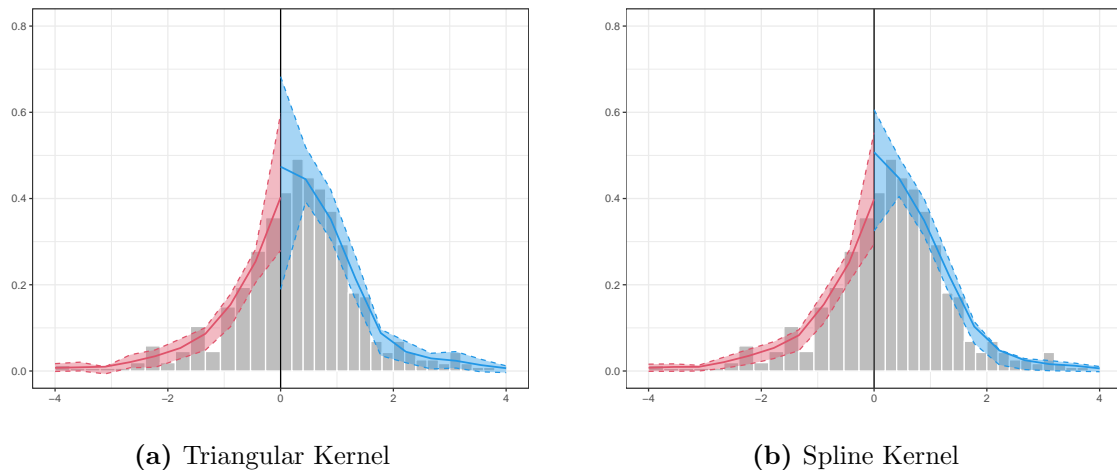


**Figure S5:** Density Test for [Eggers et al. \(2021\)](#)

## S4.5 Data Source

We list the source of the data used above. All the links are last accessed on January 27, 2024.

- Lee et al. (2004)
  - <https://github.com/scunning1975/mixtape> (Cunningham, 2021)
  - “lmb-data.dta”
- Ludwig and Miller (2007)
  - [https://github.com/rdpackages-replication/CJM\\_2020\\_JASA](https://github.com/rdpackages-replication/CJM_2020_JASA) (Cattaneo et al., 2020)
  - “headstart.csv”
- Ayres et al. (2021)
  - <https://doi.org/10.1086/715075>
  - “data\_main.dta”
- Cattaneo et al. (2023a)
  - [https://github.com/rdpackages-replication/CIT\\_2024\\_CUP](https://github.com/rdpackages-replication/CIT_2024_CUP)
  - “CIT\_2023\_CUP\_discrete.dta”
- Eggers et al. (2021)
  - <https://doi.org/10.1016/j.jmoneco.2021.03.002>
  - “mmc2.dta”

## S5 Additional Simulations

### S5.1 Main Simulation

In addition to the case when  $n = 1000, 750, 500$ , we perform the simulation for the  $n = 250$  case. The results are shown in Table S2.

### S5.2 Main Simulation under the Same Options

In the numerical experiments in the main text, we set the minimum number of observations in the bandwidth to be zero for non-compactly supported kernels. In particular, we set the options `nLocalMin=0` and `nUniqueMin=0` in `rddensity` function of Cattaneo et al. (2018, 2020). This must be natural as the local sample size consideration is not necessary for the non-compactly supported kernels. However, for transparency of our study, we report the simulation results without these specifications, i.e., we follow the original default settings of Cattaneo et al. (2018). Qualitative implications will remain.

$n$	1000			750			500			250		
Kernel	Triangular	Gaussian	Spline	Triangular	Gaussian	Spline	Triangular	Gaussian	Spline	Triangular	Gaussian	Spline
(1)	75.50	88.45	<b>96.10</b>	65.55	78.60	<b>90.65</b>	49.85	59.75	<b>73.50</b>	21.20	27.95	<b>35.55</b>
(2)	94.40	92.10	<b>97.30</b>	87.90	86.50	<b>93.85</b>	69.50	70.80	<b>82.65</b>	31.10	35.00	<b>43.85</b>
(3)	52.30	76.95	<b>94.95</b>	46.90	72.20	<b>92.10</b>	40.90	67.40	<b>87.15</b>	29.45	50.75	<b>67.55</b>
(4)	99.50	<b>100.00</b>	<b>100.00</b>	98.25	99.85	<b>100.00</b>	90.50	97.65	<b>99.95</b>	58.50	76.70	<b>91.40</b>
(5)	66.40	95.70	<b>100.00</b>	44.25	92.75	<b>99.85</b>	36.35	89.15	<b>98.75</b>	45.65	77.45	<b>89.30</b>
(6)	4.35	4.80*	4.60	4.15	4.45*	4.35	4.00	4.10*	4.05	3.95*	3.70	3.65

**Table S2:** Rejection Rates (%). The percentage of 2000 simulations with  $p$ -values below 0.05 is shown. The best for the with-manipulation cases are highlighted in bold blue. The closest to the theoretical value is marked with \* for the no-manipulation case.

$n$	1000			750			500			250		
Kernel	Triangular	Gaussian	Spline	Triangular	Gaussian	Spline	Triangular	Gaussian	Spline	Triangular	Gaussian	Spline
(1)	75.50	88.55	<b>97.60</b>	65.55	80.45	<b>92.45</b>	49.85	63.60	<b>75.00</b>	21.20	<b>35.20</b>	34.70
(2)	94.40	92.10	<b>96.90</b>	87.90	86.60	<b>89.95</b>	69.50	<b>71.65</b>	64.25	<b>31.10</b>	27.55	21.60
(3)	52.30	78.35	<b>99.60</b>	46.90	79.95	<b>99.95</b>	40.90	94.10	<b>100.00</b>	29.45	95.85	<b>97.10</b>
(4)	99.50	<b>100.00</b>	<b>100.00</b>	98.25	99.85	<b>100.00</b>	90.50	99.55	<b>99.95</b>	58.50	<b>90.00</b>	87.25
(5)	66.40	<b>100.00</b>	99.95	44.25	<b>99.80</b>	99.50	36.35	<b>98.05</b>	96.95	45.65	<b>83.00</b>	79.35
(6)	4.35	4.80*	4.75	4.15	4.55*	4.40	4.00	4.30	4.50*	3.95	4.80*	4.60

**Table S3:** Rejection Rates for Section S5.2 (%). The percentage of 2000 simulations with  $p$ -values below 0.05 is shown.

### S5.3 Discontinuity Testing using the Theoretical Bandwidths

We consider the following DGPs:

$$f_{A1}(x) = C_1 \begin{cases} \frac{8}{10} \cdot \mathcal{N}\left(-\frac{5}{2}, \left(\frac{3}{2}\right)^2\right) & x < 0 \\ \frac{12}{10} \cdot \mathcal{N}\left(1, \left(\frac{3}{2}\right)^2\right) & x \geq 0 \end{cases},$$

$$f_{A2}(x) = C_2 \begin{cases} \frac{8}{10} \cdot \mathcal{N}\left(-\frac{7}{2}, 1^2\right) & x < 0 \\ \frac{12}{10} \cdot \mathcal{N}\left(1, \left(\frac{3}{2}\right)^2\right) & x \geq 0 \end{cases},$$

where  $C_1 \simeq 1/1.65878$  and  $C_2 \simeq 1/1.69682$  are normalizing constants. The plots of these DGPs are shown in Figure S6. The density A1 exhibits a moderate-size jump at the cutoff and the density A2 shows a much larger discontinuity, like a large manipulation case.

MSE optimal bandwidth is

$$h^0(n) := h_2^{\text{MSE}} = \left( \frac{\mathcal{V}_{2,K}}{C(2,0,F)\mathcal{B}_{2,K}^2} \right)^{1/5} n^{-1/5}.$$

We use the following bandwidths: (a) Cattaneo et al. (2018, 2020)'s data-driven bandwidths  $\hat{h}_-^0$  and  $\hat{h}_+^0$ , (b) theoretical bandwidth  $h_-^0(n_-)$  and  $h_+^0(n_+)$ , and (c) theoretical bandwidth  $h_-^0(n)$  and  $h_+^0(n)$ . As in the main text, we set the minimum number of observations in the bandwidth to be zero for non-compactly supported kernels when estimating the data-driven bandwidth.

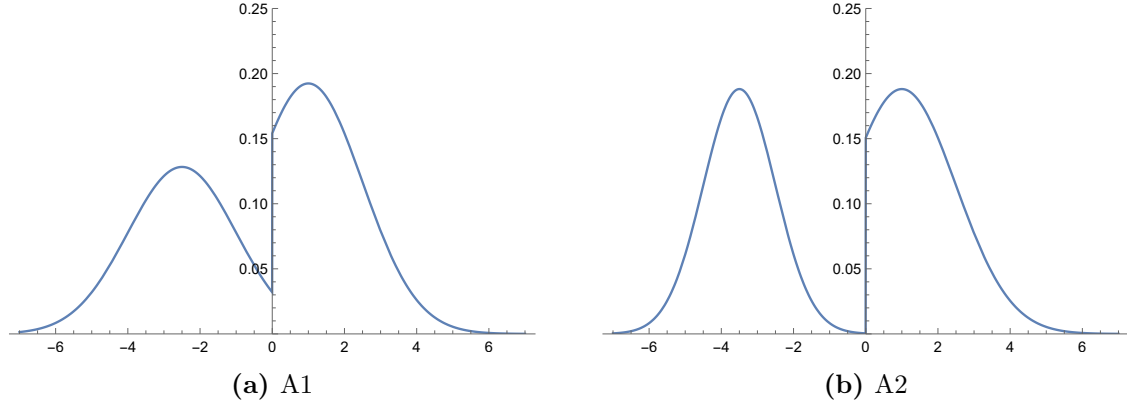


**Figure S6:** DGPs for Additional Simulation

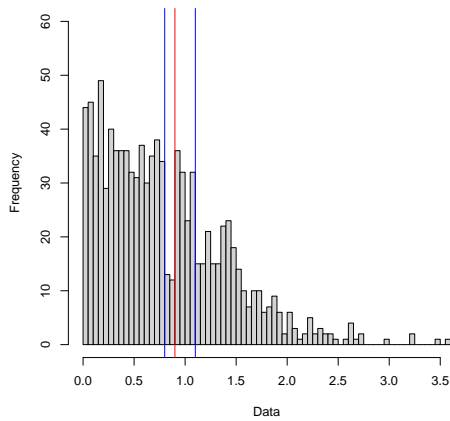
The results are summarized in Table S4. For A1, using the theoretical bandwidths leads to a certain improvement in the rejection rate for every kernel function, while the qualitative superiority of the spline-type and Gaussian kernel remains. For A2, the triangular kernel with the theoretical bandwidths does not work, as these are too small and the finite sample property dominates (Note that the data-driven bandwidth selection procedure of Cattaneo et al. (2018) are coded to choose a larger bandwidth when observations in the bandwidth are few). Regarding overall performance by the kernel, the spline-type kernel again dominates the triangular.

$n$	1000			750			500			250		
Kernel	Triangular	Gaussian	Spline	Triangular	Gaussian	Spline	Triangular	Gaussian	Spline	Triangular	Gaussian	Spline
A1-(a)	68.65	83.20	<b>95.10</b>	58.90	72.00	<b>87.75</b>	46.60	58.60	<b>74.85</b>	28.75	37.85	<b>50.10</b>
A1-(b)	86.90	93.45	<b>98.10</b>	78.00	87.30	<b>95.40</b>	61.60	72.10	<b>84.00</b>	38.90	48.20	<b>57.10</b>
A1-(c)	82.20	90.75	<b>97.15</b>	71.40	81.70	<b>91.25</b>	54.05	66.40	<b>78.45</b>	33.60	40.50	<b>50.20</b>
A2-(a)	53.55	66.20	<b>95.40</b>	38.90	51.70	<b>90.95</b>	24.35	36.75	<b>81.05</b>	10.60	18.15	<b>62.00</b>
A2-(b)	26.40	60.20	<b>90.50</b>	16.60	45.05	<b>80.00</b>	7.40	27.50	<b>63.95</b>	1.35	9.80	<b>38.70</b>
A2-(c)	12.40	48.80	<b>82.40</b>	6.90	35.10	<b>68.75</b>	2.65	20.25	<b>49.85</b>	0.55	5.30	<b>25.15</b>

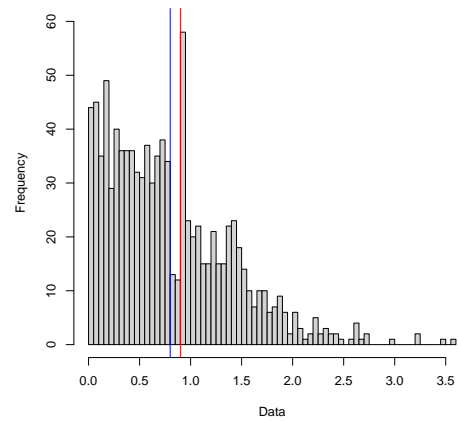
**Table S4:** Rejection Rates for Section S5.3 (%). The percentage of 2000 simulations with  $p$ -values below 0.05 is shown.

## S5.4 Histograms of the Main Simulation

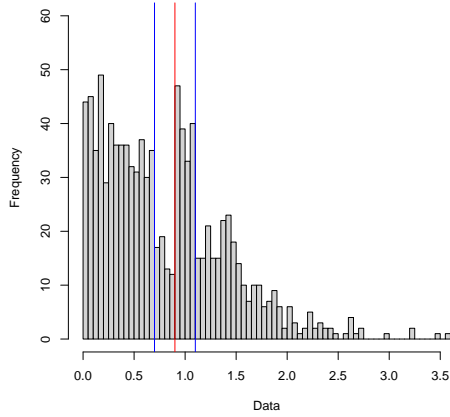
See Figure S7.



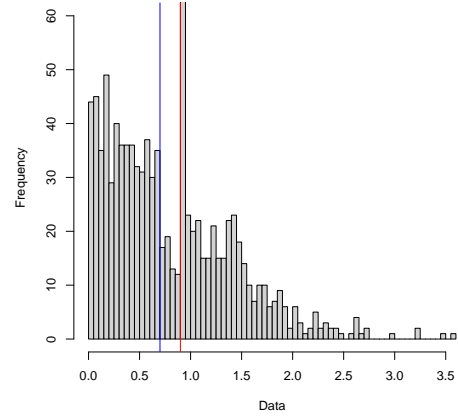
(a) Case (1)



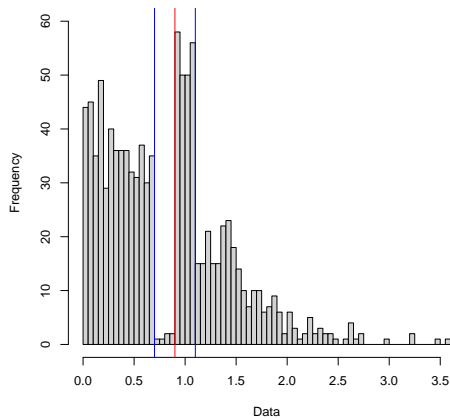
(b) Case (2)



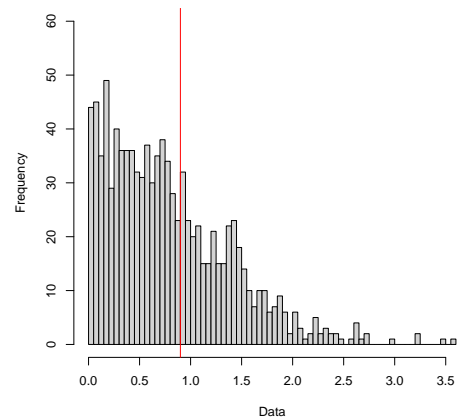
(c) Case (3)



(d) Case (4)



(e) Case (5)



(f) Case (6)

**Figure S7:** Examples of the Histogram for (1)-(6). *The red vertical line at zero indicates the cutoff. The manipulation occurs in the area between the left blue line and the red line. They move to the area below the right blue line for the case (1), (3), (5) and to the first mass point for the case (2), (4).*